3D Urban UAV Relay Placement: Linear Complexity Algorithm and Analysis

Junting Chen, *Member, IEEE*, Urbashi Mitra, *Fellow, IEEE*, and David Gesbert, *Fellow, IEEE*

***Abstract*— Optimal unmanned aerial vehicle (UAV) placement in a 3-dimensional (3D) space to build a connection between a base station (BS) and a ground user is studied herein. A key challenge is to avoid signal propagation blockage due to obstacles. Much prior work uses probabilistic terrain models with model parameters learned from the statistics over a large area, and therefore, the optimization for a specific user in a small local area is poor. In contrast, this paper seeks the optimal UAV position over *actual* and *fine-grained* terrain, and develops efficient UAV positioning strategy adaptive to the degree of location-dependent line-of-sight (LOS) condition measured on the fly. It is proven that the *globally* optimal UAV position in 3D can be determined from the proposed search trajectory which has merely linear length in the diameter of the target area. Therefore, the proposed strategy can be practically implemented. Numerical experiments are performed over a real-world urban topology and demonstrate superior performance gain over existing strategies based on probabilistic models.**

***Index Terms*— Unmanned aerial vehicle (UAV), relay networks, radio map, trajectory planning, position optimization.**

I. Introduction

LOW altitude small UAVs have great potential for boosting the performance of wireless communication networks. One trending application is to use UAVs to establish aerial relay networks [1]–[6]. Compared to traditional BSs installed at fixed positions, the UAV relay system can quickly respond to occasional and temporary service requests from a specific area in the shadow of a BS's coverage. As a result, a dynamic network can be formed to geographically track time-varying service demands and quality-of-service guarantees [7]–[10].

A compelling feature of a UAV relay system is the ability of establishing a better propagation environment for a ground user, *e.g.*, by providing LOS links. This naturally leads to the problem of optimal 3D placement of UAVs. However, since there are buildings and trees that potentially block the air-to-ground signal and create propagation shadows for the ground user, it is very challenging to find the optimal UAV position, which should depend on the propagation environment. Prior work bypassed this difficulty by using a flat-terrain model or a probabilistic terrain model to arrive at simplified problem formulations [11]–[20]. For example, [11]–[13] assumed LOS conditions regardless of the UAV and user positions. In [14]–[22], probabilistic LOS models are used, where the LOS and non-line-of-sight (NLOS) conditions are simplified into a random variable with distribution depending on the elevation angle from the user to the UAV. Since stochastic models are over-simplified, they fail to capture the actual blockage situation for a specific user. There is also a trending research direction that exploits radio maps for UAV placement to avoid the actual air-to-ground signal blockage, but existing results only optimize for the 2D case for tractable complexity, where UAVs fly at a fixed height [23], [24]. The work [25] also considered LOS-seeking online search for UAV-aided free space optical communication, but the method is limited to 2D case.

The goal of the paper is to develop fine-grained *blockage-aware* algorithms for the online search of the optimal UAV position in 3D. There are two main challenges: the sampling complexity for acquiring the propagation conditions and the computational complexity due to the unstructured terrain. First, if there is no radio map available, the UAV may need to spend a tremendous amount of flight time to explore every propagation opportunity in 3D. However, an exhaustive search is prohibitive due to the very limited UAV flight time. Second, even if we store the entire radio map in an offline database, the computation for the optimal UAV position is still very expensive for real time applications because the obstacles may have arbitrary shapes and so as the patterns of the radio maps.

Our approach is to exploit the hidden structure of the propagation from a direct ray-tracing mechanism: First, if the UAV-user link is in LOS, then it remains in LOS when

Manuscript received August 11, 2020; revised November 27, 2020 and January 26, 2021; accepted March 3, 2021. Date of publication March 23, 2021; date of current version August 12, 2021. This work was supported in part by the National Key Research and Development Program of China under Grant 2018YFB1800800; in part by the Key Area Research and Development Program of Guangdong Province under Grant 2018B030338001; in part by the Shenzhen Outstanding Talents Training Fund, Guangdong Research, under Project 2017ZT07X152; in part by the Shenzhen Institute of AIRS under Grant AC01202005001; in part by the Guangdong Fund under Grant 2019QN01X895; in part by Office of Naval Research (ONR) under Grant N00014-15-1-2550, Grant NSF CNS-1213128, Grant NSF CCF-1718560, Grant NSF CCF-1410009, Grant NSF CPS-1446901, and Grant AFOSR A9550-12-1-0215; and in part by the European Research Council (ERC) under European Union Horizon 2020 research and innovation program under Grant 670896. The associate editor coordinating the review of this article and approving it for publication was B. Smida. *(Corresponding author: Junting Chen.)*

Junting Chen is with the Future Network of Intelligence Institute (FNii) and the School of Science and Engineering, The Chinese University of Hong Kong, Shenzhen 518172, China (e-mail: juntingc@cuhk.edu.cn).

Urbashi Mitra is with the Ming Hsieh Department of Electrical Engineering, University of Southern California, Los Angeles, CA 90089 USA (e-mail: ubli@usc.edu).

David Gesbert is with the Department of Communication Systems, EURECOM, 06410 Sophia-Antipolis, France (e-mail: gesbert@eurecom.fr).

Color versions of one or more figures in this article are available at https://doi.org/10.1109/TWC.2021.3066429.

Digital Object Identifier 10.1109/TWC.2021.3066429

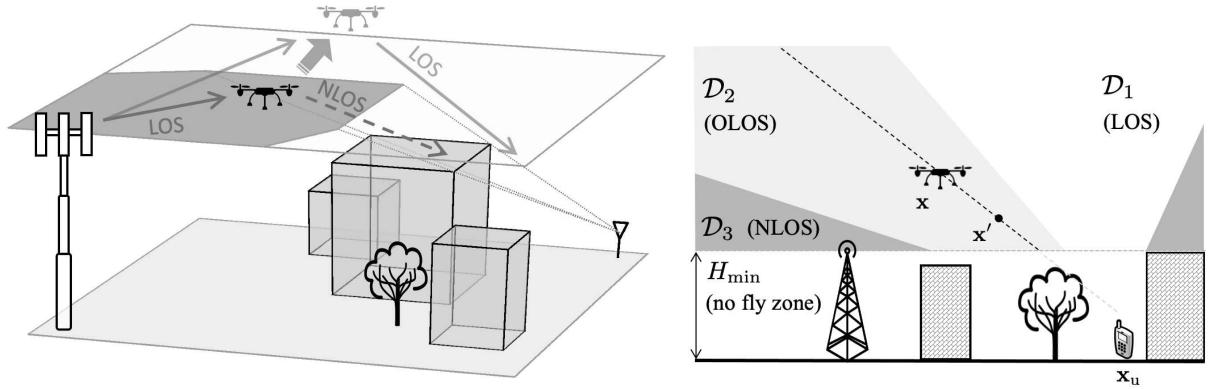

(a) UAV relay network (b) Multi-segment propagation model

Fig. 1. (a) The UAV may adjust its position in 3D to avoid signal blockage (grey area) from the user. (b) Multi-segment propagation model: (1) When the UAV moves upwards, it will experience a smaller degree of obstruction; (2) When the UAV moves along the black dashed line, it travels along the same propagation segment (*i.e.*, same degree of obstruction).

the UAV moves closer to the user, whereas, when it is in NLOS, it remains in NLOS when the UAV moves away (see Fig. 1-(b)). Second, when the elevation angle from the user to the UAV increases, the degree of LOS obstruction tends to decrease. Existing work has leveraged the stochastic version of these features to arrive at probabilistic LOS models for UAV placement [14]–[22]. Herein, we show that exploiting the *deterministic* version of these features can achieve a much higher performance gain, since the UAV has a better sense of the environment. We develop an *exploration-and-exploitation* search strategy with only *linear* search complexity. Somewhat surprisingly, it can be proven that the proposed search leads to the *global optimal* solution under mild conditions. This result theoretically justifies the substantial performance gain of the proposed method. Our prior work [9] studied a similar UAV positioning problem in 2D by assuming a fixed UAV height, but such a constraint limits the potential gain of the UAV relay system. The extension to 3D requires a new design of the strategy for low complexity search.

To summarize, the contributions of this paper are:

- We develop a search strategy to find the optimal the UAV position in 3D that is aware of the fine-grained actual propagation environment for the target user. The worst-case search length is linear in the diameter of the target area.
- We prove that the search algorithm finds the globally optimal UAV position over arbitrary terrain structures, providing theoretical justification for the proposed strategy.
- We evaluate the proposed strategy for three UAV application examples over a real-world urban city topology, demonstrating substantial performance gain over the state-of-the-art solutions, such as the methods based on probabilistic LOS models.

The rest of the paper is organized as follows. Section II presents the segmented propagation model and the problem formulation. Section III develops an angular coordinate transformation to enable an effective search on a 2D plane. The algorithm is then described in Section IV with optimality and complexity analysis. Three application examples are formulated in Section V with numerical evaluation over an actual topology in Section VI. Finally, Section VII provides the conclusions.

TABLE I
KEY NOTATIONS

Symbols	Meaning
$\mathbf{x}$, $\mathbf{x}_u$, $\mathbf{x}_b$	The positions in 3D of the UAV, user, and BS, respectively (Section II).
$\bar{\mathbf{x}}_s$	The point on the 2D horizontal plane $x_3 = H_s$ such that $\mathbf{x}$, $\mathbf{x}_u$, and $(\bar{\mathbf{x}}_s, H_s)$ are collinear (Section III-A).
$\bar{\mathbf{x}}$, $\bar{\mathbf{x}}_u$, $\bar{\mathbf{x}}_b$	The points where $\mathbf{x}$, $\mathbf{x}_u$, and $\mathbf{x}_b$ are, respectively, projected on the 2D plane $x_3 = H_s$ (Section III-A).
$d_u(\mathbf{x})$, $d_b(\mathbf{x})$	Distances from the UAV at $\mathbf{x}$ to the user $\mathbf{x}_u$ and BS $\mathbf{x}_b$, respectively (Section II-A).
$\mathcal{D}_k$	The set of UAV locations $\mathbf{x}$ such that the UAV-user link is in the kth propagation region (Section II-A).
$f_k(d_u, d_b)(\mathbf{x})$	The system cost function when the UAV locates in the kth propagation region $\mathcal{D}_k$ (Section II-B).
$\tilde{f}_k(l, \rho, \theta)$	The same cost function f_k expressed using the angular coordinate (l, ρ, θ) (Section III-B).
$F_k(\rho, \theta)$	The cost function $\tilde{f}_k(l^*(\rho, \theta), \rho, \theta)$ where the variable l has been optimized (Section III-B).
$\mathcal{P}_k$	The set of UAV positions on $x_3 = H_s$ using the (ρ, θ)-coordinates such that $\mathbf{x} \in \mathcal{D}_k$ (Definition 2).

Notation: For functions $g_1(\mathbf{x}), g_2(\mathbf{x}), \ldots, g_M(\mathbf{x}) : \mathbb{R}^m \mapsto \mathbb{R}$ and a function $f(g_1, g_2, \ldots, g_M) : \mathbb{R}^M \to \mathbb{R}$, the form $f(g_1, g_2, \ldots, g_M)(\mathbf{x})$ is a short-hand notation of the composite function $f(g_1(\mathbf{x}), g_2(\mathbf{x}), \ldots, g_M(\mathbf{x}))$. Other key notations are summarized in Table I.

II. System Model

Consider a BS located at $\mathbf{x}_b \in \mathbb{R}^3$ and a user located at $\mathbf{x}_u \in \mathbb{R}^3$ which is in the propagation shadow of the BS. A UAV is employed to relay the signal between the BS and the user. The user location is fixed and the UAV position $\mathbf{x} = (x_1, x_2, x_3) \in \mathbb{R}^3$ is to be optimized. Suppose that the altitude of the UAV is lower bounded by $H_{\min}$, the height of the tallest building, such that no collision will occur. In addition, assume that the

BS is placed on a high enough tower, and therefore, there is always an LOS condition between the UAV and the BS. However, the UAV-user link likely gets obstructed as shown in Fig. 1-(a).

A. Channel and Environment Models

Since the UAV position will be optimized in a relatively large timescale, we focus on the adaptation to the large-scale channel characteristics. The BS-UAV channel in decibel is modeled as $[g_{\mathrm{b}}(\mathbf{x})]_{\mathrm{dB}} = b_0 - a_0 \log_{10} d_{\mathrm{b}}(\mathbf{x})$ as LOS is always assumed for the BS-UAV link, where $d_{\mathrm{b}}(\mathbf{x}) \triangleq \|\mathbf{x} - \mathbf{x}_{\mathrm{b}}\|_2$ is the UAV-BS distance.

On the other hand, the UAV-user link can be modeled as

$$[g_{\mathrm{u}}(\mathbf{x})]_{\mathrm{dB}} = \begin{cases} b_1 - a_1 \log_{10} d_{\mathrm{u}}(\mathbf{x}) + \xi_1, & \text{LOS} \\ b_2 - a_2 \log_{10} d_{\mathrm{u}}(\mathbf{x}) + \xi_2, & \text{NLOS} \end{cases} \quad (1)$$

where $d_{\mathrm{u}}(\mathbf{x}) \triangleq \|\mathbf{x} - \mathbf{x}_{\mathrm{u}}\|_2$ is the UAV-user distance, a_k and b_k are the path loss parameters, and ξ_k are random variables to capture the shadowing. Conventionally, LOS is defined as the scenario where the direct propagation path is not obstructed; otherwise, the link is in NLOS.

In a more general setting, the system may have the ability to identify multiple degrees of LOS obstruction. We extend the classical channel model (1) to the K-segment case. Define $\mathcal{D}_k$ as the set of UAV locations in which the direct path of the UAV-user link experiences *degree*-$(k-1)$ of LOS obstruction as shown in Fig. 1. As a result, UAV-user channel in a large timescale can be written as

$$[g_{\mathrm{u}}(\mathbf{x})]_{\mathrm{dB}} = \sum_{k=1}^{K} (b_k - a_k \log_{10} d_{\mathrm{u}}(\mathbf{x}) + \xi_k) \mathbb{I}\{\mathbf{x} \in \mathcal{D}_k\} \quad (2)$$

where $\mathbb{I}\{A\}$ is an indicator function taking value 1 if condition A is satisfied, and 0 otherwise. Intuitively, the more propagation regions $\mathcal{D}_k$ to identify, the smaller the variance of ξ_k, which captures the residual shadowing due to reflection and diffraction. Such an observation was experimentally validated in [26] and [27].

In addition, we impose two regularization conditions to shape $\mathcal{D}_k$ as shown in Fig. 1-(b):

A1) Increasing the altitude of the UAV will lower the degree of LOS obstruction, and

A2) The feasible UAV positions that are in line with a given user position are in the same propagation region.

An illustrative example is given in Fig. 1-(b), where, for a user at $\mathbf{x}_{\mathrm{u}}$, all UAV positions on the dashed ray belong to obstructed line-of-sight (OLOS). On the other hand, if the UAV increases its altitude from the dashed line, it may enter LOS. Note that any channel measurement data can be fit to model (2) with conditions II-A and II-A imposed.

We do not make any assumption on the statistics of ξ_k in (2), but we assume that the propagation condition $\mathbb{I}\{\mathbf{x} \in \mathcal{D}_k\}$ can be perfectly determined along the search path $\mathbf{x}(t)$ of the UAV. In practice, hypothesis testing or other statistical learning methods can be applied to determine $\mathbb{I}\{\mathbf{x} \in \mathcal{D}_k\}$ from the measurement data [9], [28], [29].

B. Problem Formulation

We explain our general formulation from an example, where a UAV serves as a relay that employs a decode-and-forward strategy to connect the BS with the user. One may wish to maximize the end-to-end capacity[1]

$$-f(\mathbf{x}) \triangleq \min \Big\{ \log_2(1 + \kappa_{\mathrm{b}} \mathbb{E}\{g_{\mathrm{b}}(\mathbf{x})\}), \log_2(1 + \kappa_{\mathrm{u}} \mathbb{E}\{g_{\mathrm{u}}(\mathbf{x})\}) \Big\} \quad (3)$$

where the expectation is taken over the randomness of the residual shadowing ξ_k, and hence, $\mathbb{E}\{g_{\mathrm{b}}(\mathbf{x})\}$ and $\mathbb{E}\{g_{\mathrm{b}}(\mathbf{x})\}$ give the average signal-to-noise ratio (SNR). The first term in (3) captures the approximate spectrum efficiency of the UAV-BS link and the second term captures that of the UAV-user link, in which, the parameters κ_{u} and κ_{b} characterize the SNR back off due to the discrete transmission power control, the discrete choice of modulation schemes, coding loss, small-scale fading and shadowing statistics, *etc*. In (3), the cost only depends on the distance $d_{\mathrm{b}}(\mathbf{x})$ or $d_{\mathrm{u}}(\mathbf{x})$ and the LOS condition $\mathbb{I}\{\mathbf{x} \in \mathcal{D}_k\}$. As a result, (3) can be equivalently written as a decomposable form $f(\mathbf{x}) = \sum_{k=1}^{K} f_k(d_{\mathrm{u}}(\mathbf{x}), d_{\mathrm{b}}(\mathbf{x})) \mathbb{I}\{\mathbf{x} \in \mathcal{D}_k\}$, where the sub-function f_k corresponds to the objective $f(\mathbf{x})$ in (3) evaluated under the condition that the UAV locates in the kth propagation region $\mathcal{D}_k$, *i.e.*, $\mathbb{I}\{\mathbf{x} \in \mathcal{D}_k\} = 1$.

It is important to note that in (3), the objective $f(\mathbf{x})$ is discontinuous in $\mathbf{x}$ due to the indicator function in (2), whereas, the sub-functions f_k's are continuous in $\mathbf{x}$.

Similar to the above example, many UAV positioning problems can be formulated into the following general form:

$$\mathscr{P}: \ \underset{\mathbf{x} \in \mathbb{R}^3}{\text{minimize}} \ \sum_{k=1}^{K} f_k(d_{\mathrm{u}}, d_{\mathrm{b}})(\mathbf{x}) \mathbb{I}\{\mathbf{x} \in \mathcal{D}_k\} \quad \text{subject to } H_{\min} \le x_3 \le H_{\max} \quad (4)$$

where $f_k(z, y)(\mathbf{x})$ is a short-hand notation for $f_k(z(\mathbf{x}), y(\mathbf{x}))$, which is the specific cost if the link is in the kth propagation condition. The constant $H_{\min}$ is assumed to be larger than the height of the tallest building.

Finally, it is natural to assume that the cost sub-functions f_k satisfy the following two mild conditions:

A3) The cost f_k for each propagation segment k is non-decreasing with the distances d_{u} and d_{b}, respectively,

A4) The cost in a less obstructed region is smaller than the one in a more obstructed region:

$$f_k(d_{\mathrm{u}}, d_{\mathrm{b}})(\mathbf{x}) \le f_{k+1}(d_{\mathrm{u}}, d_{\mathrm{b}})(\mathbf{x}) \quad (5)$$

for $k = 1, 2, \ldots, K-1$.

It can be easily verified that the example formulation (3) satisfies these two conditions.

[1]The negative sign is because we want to unify our formulation as minimizing a "cost" function.

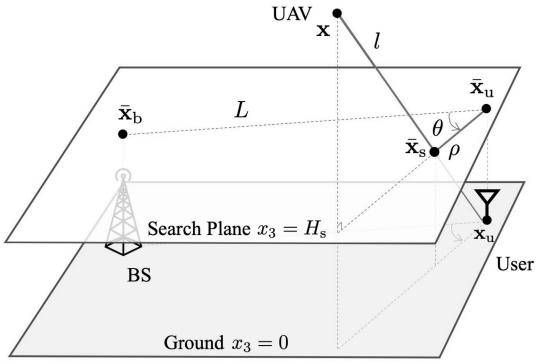

Fig. 2. Geometric interpretation of the angular transformation. The coordinate $(\bar{\mathbf{x}}_\mathrm{s}, H_\mathrm{s})$ on the search plane $x_3 = H_\mathrm{s}$ is transformed to (ρ, θ).

III. Design of the Algorithm

In this section, we first show that, to find the optimal position in 3D, it suffices to search on a 2D horizontal plane $x_3 = H_\mathrm{s}$ under an arbitrary altitude H_s, $H_\mathrm{min} \le H_\mathrm{s} \le H_\mathrm{max}$. The intuition is that, if the UAV position $\mathbf{x}$ is known to belong to $\mathcal{D}_2$, then all the positions along the dashed line are in $\mathcal{D}_2$ (see Fig. 1-(b)), and hence, the UAV need not explore the entire dashed line.

To exploit such a property, this section first develops an angular coordinate system (l, ρ, θ), and then, shows how to transform the 3D cost functions $f_k(\mathbf{x})$ into 2D *proxy* segment cost functions $F_k(\rho, \theta)$ by first optimizing over l. Finally, based on $F_k(\rho, \theta)$, a low complexity search strategy is developed to find the optimal position in 3D.

A. Angular Coordinate System

Recall that $\mathbf{x}$, $\mathbf{x}_\mathrm{u}$, and $\mathbf{x}_\mathrm{b}$ represent the UAV position, the user position and the BS position, respectively, in 3D. As shown in Fig. 2, Let $(\bar{\mathbf{x}}_\mathrm{s}, H_\mathrm{s})$ be the point where the line segment joining $\mathbf{x}$ and $\mathbf{x}_\mathrm{u}$ intersects with the search plane $x_3 = H_\mathrm{s}$, *i.e.*, $\bar{\mathbf{x}}_\mathrm{s} \in \mathbb{R}^2$ is a point on the $x_3 = H_\mathrm{s}$ plane such that the three points $\mathbf{x}$, $\mathbf{x}_\mathrm{u}$, and $(\bar{\mathbf{x}}_\mathrm{s}, H_\mathrm{s})$ are collinear. In addition, denote $(\bar{\mathbf{x}}, H_\mathrm{s})$, $(\bar{\mathbf{x}}_\mathrm{u}, H_\mathrm{s})$, and $(\bar{\mathbf{x}}_\mathrm{b}, H_\mathrm{s})$ as the points where $\mathbf{x}$, $\mathbf{x}_\mathrm{u}$, and $\mathbf{x}_\mathrm{b}$ are projected on the search plane $x_3 = H_\mathrm{s}$, respectively. Denote $l \triangleq \|\mathbf{x} - \mathbf{x}_\mathrm{u}\|_2$, $\rho \triangleq \|\bar{\mathbf{x}}_\mathrm{s} - \bar{\mathbf{x}}_\mathrm{u}\|_2$, and θ as the angle from vector $\bar{\mathbf{x}}_\mathrm{b} - \bar{\mathbf{x}}_\mathrm{u}$ to vector $\bar{\mathbf{x}}_\mathrm{s} - \bar{\mathbf{x}}_\mathrm{u}$. One can verify that the UAV position $\mathbf{x} = (x_1, x_2, x_3)$ can be uniquely represented by the angular coordinates (l, ρ, θ).

Using the geometric relation, the transformation from (x_1, x_2, x_3) to (l, ρ, θ) is:

$$l(\mathbf{x}) = \|\mathbf{x} - \mathbf{x}_\mathrm{u}\|_2 \tag{6}$$

$$\rho(\mathbf{x}) = \frac{H_\mathrm{s}}{x_3}\|\bar{\mathbf{x}} - \bar{\mathbf{x}}_\mathrm{u}\|_2 \tag{7}$$

$$\theta(\mathbf{x}) = \mathrm{sign}(z_2 u_1 - z_1 u_2) \cdot \arccos\left(\mathbf{z}^\mathrm{T}\mathbf{u}/\|\mathbf{z}\|\right) \tag{8}$$

where $\mathbf{z} = (z_1, z_2) \triangleq \bar{\mathbf{x}} - \bar{\mathbf{x}}_\mathrm{u}$, $\mathbf{u} = (u_1, u_2) \triangleq (\bar{\mathbf{x}}_\mathrm{b} - \bar{\mathbf{x}}_\mathrm{u})/\|\bar{\mathbf{x}}_\mathrm{b} - \bar{\mathbf{x}}_\mathrm{u}\|$ is the reference direction pointing from $\bar{\mathbf{x}}_\mathrm{u}$ to $\bar{\mathbf{x}}_\mathrm{b}$, and $\mathrm{sign}(x) = 1$ if $x > 0$, and $\mathrm{sign}(x) = -1$, otherwise.

In turn, the transformation from the angular coordinates (l, ρ, θ) to the Cartesian coordinates $\mathbf{x} = (x_1, x_2, x_3)$ can be computed as

$$\mathbf{x}(l, \rho, \theta) = l\frac{(\bar{\mathbf{x}}_\mathrm{s}(\rho, \theta), H_\mathrm{s}) - \mathbf{x}_\mathrm{u}}{\|(\bar{\mathbf{x}}_\mathrm{s}(\rho, \theta), H_\mathrm{s}) - \mathbf{x}_\mathrm{u}\|} \tag{9}$$

where $\bar{\mathbf{x}}_\mathrm{s}(\rho, \theta) = \bar{\mathbf{x}}_\mathrm{u} + \rho\mathbf{M}(\theta)\mathbf{u}$, and

$$\mathbf{M}(\theta) = \begin{bmatrix} \cos\theta & -\sin\theta \\ \sin\theta & \cos\theta \end{bmatrix}$$

is a rotation matrix.

B. The Proxy Cost Function on the 2D Search Plane

Given the propagation condition observed at the search position $(\bar{\mathbf{x}}_\mathrm{s}(\rho, \theta), H_\mathrm{s})$, the cost at every l can be mathematically computed, since they are under the same propagation condition according to property II-A as illustrated in Fig. 1-(b).

In the following, we define the *proxy segment cost* $F_k(\rho, \theta)$ on the 2D search plane by first transforming $f_k(\mathbf{x})$ to $\tilde{f}_k(l, \rho, \theta)$ using the coordinate transform and then minimizing $\tilde{f}_k(l, \rho, \theta)$ over l.

First, using the coordinate transformation (6)–(8), problem $\mathscr{P}$ can be equivalently written in the form of (l, ρ, θ) as

$$\mathscr{P}': \quad \underset{\rho \ge 0, \theta \in (-\pi, \pi), l \in \mathcal{L}(\rho)}{\text{minimize}} \sum_{k=1}^{K} \tilde{f}_k(l, \rho, \theta)\mathbb{I}\{\mathbf{x}(l, \rho, \theta) \in \mathcal{D}_k\}$$

where $\tilde{f}_k(l, \rho, \theta) \triangleq f_k(d_\mathrm{u}, d_\mathrm{b})(\mathbf{x}(l, \rho, \theta))$ and

$$\mathcal{L}(\rho) = \left\{ l : \frac{H_\mathrm{min}}{H_\mathrm{s}}\sqrt{\rho^2 + H_\mathrm{s}^2} \le l \le \frac{H_\mathrm{max}}{H_\mathrm{s}}\sqrt{\rho^2 + H_\mathrm{s}^2} \right\}. \tag{10}$$

Second, observed that problem $\mathscr{P}'$ can be decomposed into an inner problem

$$\underset{l \in \mathcal{L}(\rho)}{\text{minimize}} \quad \sum_{k=1}^{K} \tilde{f}_k(l, \rho, \theta)\mathbb{I}\{\mathbf{x}(l, \rho, \theta) \in \mathcal{D}_k\} \tag{11}$$

which minimizes over l and an outer problem which minimizes over ρ and θ. Given (ρ, θ), the inner problem can be further written into K subproblems each minimizing $\tilde{f}_k(l, \rho, \theta)$ over l.

Let

$$l_k^*(\rho, \theta) \triangleq \underset{l \in \mathcal{L}(\rho)}{\arg\min} \quad \tilde{f}_k(l, \rho, \theta) \tag{12}$$

be the solution to the kth inner subproblem of $\mathscr{P}'$. In the example shown in Fig. 1-(b), $l_k^*(\rho, \theta)$ corresponds to the local optimal position along the black dashed line, with (ρ, θ) being the coordinate obtained from (7)–(8) for a given $\mathbf{x}$.

The cost evaluated at local optimal point $(l_k^*(\rho, \theta), \rho, \theta)$ for the kth propagation condition is then defined as the *proxy segment cost* $F_k(\rho, \theta)$ as follows.

Definition 1 (Proxy Segment Cost): The proxy cost for the kth segment is defined as

$$F_k(\rho, \theta) \triangleq \tilde{f}_k(l_k^*(\rho, \theta), \rho, \theta). \tag{13}$$

In addition, the *proxy cost* $F(\rho, \theta)$ on the 2D search plane is defined as follows.

Definition 2 (Proxy Cost): The proxy cost at the search coordinate (ρ,θ) on the search plane is defined as

$$F(\rho,\theta) \triangleq \sum_{k=1}^{K} F_k(\rho,\theta)\mathbb{I}\{(\rho,\theta)\in\mathcal{P}_k\} \tag{14}$$

where $\mathcal{P}_k \triangleq \big\{(\rho,\theta) : \mathbf{x}(l^*(\rho,\theta),\rho,\theta)\in\mathcal{D}_k\big\}$ is the kth propagation segment expressed in the angular coordinate system.

The following establishes the connection between the proxy segment cost $F_k(\rho,\theta)$ and the segment cost $F(\rho,\theta)$.

Proposition 1: Given (ρ,θ) to examine the propagation condition at an arbitrary position $l\in\mathcal{L}(\rho)$. If $\mathbf{x}(l,\rho,\theta)\in\mathcal{D}_{\hat{k}}$ for some $\hat{k}$, then, $F(\rho,\theta)=F_{\hat{k}}(\rho,\theta)$.

Proof: Define $l^*(\rho,\theta)$ as the solution to the inner subproblem (11) of $\mathscr{P}'$. Property II-A and our construction of the angular coordinate system imply that, given a fixed search coordinate (ρ,θ), all possible UAV positions $\mathbf{x}(l,\rho,\theta)$ belongs to the same propagation condition $\mathbf{x}(l,\rho,\theta)\in\mathcal{D}_{\hat{k}}$ for some $\hat{k}$. This property justifies that $l^*(\rho,\theta)=l^*_{\hat{k}}(\rho,\theta)$. As a result, $\mathbb{I}\{(\rho,\theta)\in\mathcal{P}_{\hat{k}}\}=\mathbb{I}\{\mathbf{x}(l^*,\rho,\theta)\in\mathcal{D}_{\hat{k}}\}=\mathbb{I}\{\mathbf{x}(l^*_{\hat{k}},\rho,\theta)\in\mathcal{D}_{\hat{k}}\}$, and hence, $F(\rho,\theta)=F_{\hat{k}}(\rho,\theta)$. □

Following the above property, problem $\mathscr{P}'$ can be further transformed into a 2D search problem

$$\mathscr{P}'': \quad \underset{\rho\geq 0,\,-\pi\leq\theta\leq\pi}{\text{minimize}} \quad F(\rho,\theta)$$

which drives the following algorithm design.

C. Algorithm Design

The main idea of the search strategy is described as follows with full technical details given in Algorithm 1.

1) $K=2$ Case: In the two segment case, the algorithm performs in two phases. In phase 0, the UAV starts from the BS location $\bar{\mathbf{x}}_{\rm b}$ and moves towards the user at $\bar{\mathbf{x}}_{\rm u}$ on the search plane $x_3=H_{\rm s}$, until it detects the LOS and NLOS boundary. The search then enters to phase 1.

In phase 1, the UAV moves according to the two possible conditions it detects. If it is in the LOS segment, it moves away from the user by increasing ρ until the new position does not decrease the proxy segment cost $F_1(\rho,\theta)$ any more or until the UAV enters in NLOS. If it is in the NLOS segment, it moves along the contour specified by $F_1(\rho,\theta)=$ constant. The search continues until the stopping criterion is met, *i.e.*, either $\rho\geq\frac{H_{\rm s}}{H_{\min}}\cos\theta\|\bar{\mathbf{x}}_{\rm b}-\bar{\mathbf{x}}_{\rm u}\|_2$ or $\partial F_k(\rho,\theta)/\partial\rho\geq 0$, or until the UAV enters in the LOS as illustrated in Fig. 3. The stopping criteria will be explained in Section IV.

2) $K>2$ Case: For the multiple propagation segment case, the algorithm has K phases. In the kth phase, the segment $\bigcup_{j=1}^{k}\mathcal{D}_i$ (or $\bigcup_{j=1}^{k}\mathcal{P}_i$ in the polar domain) is treated as a *virtual* LOS segment, and the rest is treated as a *virtual* NLOS segment. The UAV follows the search strategy specified in phase 1 of the $K=2$ case until the stopping criterion is met. It will be shown in Section IV-C that when the whole algorithm terminates, the globally optimal UAV position must have been visited by the trajectory that the UAV has visited.

Algorithm 1 Search Strategy for the Optimal UAV Position

Choose a step size $\delta>0$. The search is carried out on a 2D search plane $x_3=H_{\rm s}$ using the coordinates (ρ,θ) defined in (6)–(8).

1) **Search along $\theta=0$:** Find the critical points ρ_k^0, $k=1,2,\ldots,K$, defined as the solution to
$$\underset{\rho\geq 0,\ (\rho,0)\in\bigcup_{j=1}^{k}\mathcal{P}_j}{\text{minimize}} \quad F_k(\rho,0) \tag{15}$$
Initialize $F_{\min}=F_1(\rho_1^0,0)$, $(\hat{\rho},\hat{\theta})=(\rho_1^0,0)$, and $k=1$.
2) **Search on the right branch:** Set $(\rho,\theta)\leftarrow(\rho_k^0,\delta/\rho_k^0)$.
3) Proceed according to the following two statuses
   a) **Virtual LOS:** If $(\rho,\theta)\in\bigcup_{j=1}^{k}\mathcal{P}_j$, update according to
   $$\rho\leftarrow\rho+\delta. \tag{16}$$
   If $F_k(\rho,\theta)<F_{\min}$, then update the record $F_{\min}\leftarrow F_k(\rho,\theta)$ and $(\hat{\rho},\hat{\theta})\leftarrow(\rho,\theta)$.
   b) **Virtual NLOS:** If $(\rho,\theta)\in\bigcup_{j=k+1}^{K}\mathcal{P}_j$, update according to
   $$\rho\leftarrow\rho+\gamma,\ \theta\leftarrow\theta+\gamma\Big(-\frac{\partial F_k}{\partial\theta}\Big)^{-1}\frac{\partial F_k}{\partial\rho} \tag{17}$$
   where $\gamma>0$ is chosen such that the UAV position change satisfy the step size $\|\Delta\bar{\mathbf{x}}_{\rm s}\|_2=\delta$.
   Repeat this step until either (i) $\rho\geq\frac{H_{\rm s}}{H_{\min}}L\cos\theta$ or (ii) $\partial F_k(\rho,\theta)/\partial\rho\geq 0$, where $L\triangleq\|\bar{\mathbf{x}}_{\rm b}-\bar{\mathbf{x}}_{\rm u}\|_2$.
4) **Search on the left branch:** Set $(\rho,\theta)\leftarrow(\rho_k^0,-\delta/\rho_k^0)$. Repeat from Step 3).
5) Let $k\leftarrow k+1$. Repeat from Step 2) until $k>K-1$.
6) If $F_K(\rho_K^0,0)<F_{\min}$, then $F_{\min}\leftarrow F_K(\rho_K^0,0)$ and $(\hat{\rho},\hat{\theta})\leftarrow(\rho_K^0,0)$.

The optimal position is given by $\mathbf{x}(l^*(\hat{\rho},\hat{\theta}),\hat{\rho},\hat{\theta})$ from (9).

D. Detecting Propagation Segment

Algorithm 1 requires detection on the propagation segment $\mathbf{x}\in\mathcal{D}_k$ along the search trajectory $\mathbf{x}$. In practice, the detection can be realized using a maximum likelihood estimation method. For the kth propagation segment, let $h_k(u)$ be the probability density function of the random variable ξ_k in the model (2). Then, given the channel gain measurement y in decibel at UAV location $\mathbf{x}$, one can pick propagation segment $\hat{k}$ that maximizes the likelihood function

$$\hat{k}=\underset{k=1,2,\ldots,K}{\text{argmax}}\ h_k(y-b_k+a_k\log_{10}d_{\rm u}(\mathbf{x})).$$

In particular, if ξ_k is further modeled as a Gaussian random variable with variance σ_k^2, then, the detection rule can be further derived as

$$\hat{k}=\underset{k=1,2,\ldots,K}{\text{argmin}}\ \frac{1}{\sigma_k}\left|y-b_k+a_k\log_{10}d_{\rm u}(\mathbf{x})\right|.$$

The above detection method implicitly assumes the knowledge of propagation parameters a_k, b_k, and σ_k, which can be obtained either from a separate training phase or from Step 1 in Algorithm 1. In the latter case, the UAV first searches on

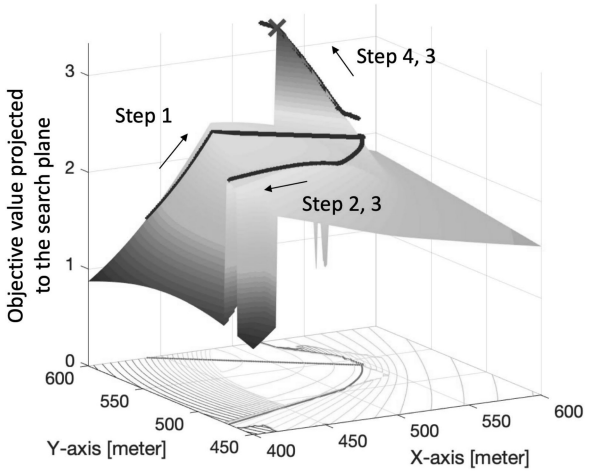

(a)

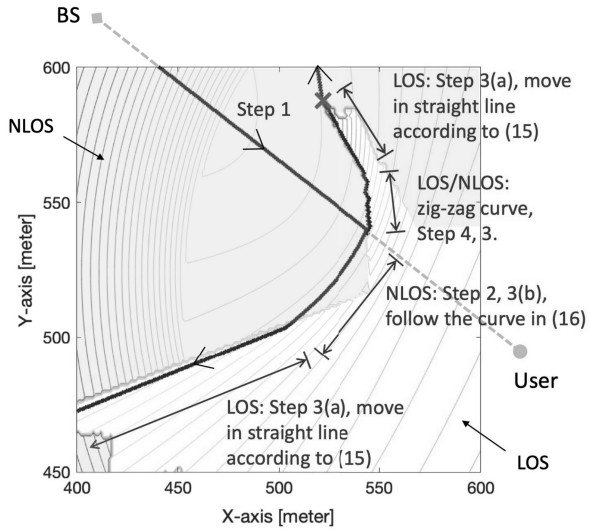

(b)

Fig. 3. (a) The running best objective value (projected to the search plane) discovered along the search path, the black curve. (b) The corresponding search path on the search plane.

the BS-user axis to collect channel measurements, and then performs parameter estimation for a_k, b_k, and σ_k [28], [30].

IV. Complexity and Optimality Analysis

In this section, we focus on the algorithm analysis for two types of cost functions $f_k(x, y)$:

Type I. For every $x, y > 0$, $f_k(x, y) > 0$, $\frac{\partial f_k(x,y)}{\partial x}, \frac{\partial f_k(x,y)}{\partial y} > 0$, $\frac{\partial^2 f_k(x,y)}{\partial x \partial y} = 0$, and

$$\frac{\partial^2 f_k(x,y)}{\partial x^2} - \frac{1}{x}\frac{\partial f_k(x,y)}{\partial x} \geq 0 \tag{18}$$

$$\frac{\partial^2 f_k(x,y)}{\partial y^2} - \frac{1}{y}\frac{\partial f_k(x,y)}{\partial y} \geq 0. \tag{19}$$

Type II. There exist continuous, positive, and strictly increasing functions $f_k^{(1)}(x)$ and $f_k^{(2)}(y)$ for $x, y > 0$, such that

$$f_k(x, y) = \max\{f_k^{(1)}(x), f_k^{(2)}(y)\}. \tag{20}$$

Note that convexity is not required, and recall that, in our formulation $\mathscr{P}$, the arguments x and y in $f_k(x, y)$ correspond to the distances $d_{\mathrm{u}}(\mathbf{x})$ and $d_{\mathrm{b}}(\mathbf{x})$, respectively. These two types of cost functions have a vast of applications as will be seen in Section V. Examples of Type I functions include the outage probability as a function of path loss with respect to (w.r.t.) the distances in a relay channel [31], [32]. Examples of Type II functions are the end-to-end ergodic capacity (with a negative sign) of a relay channel [32], [33].

A. Unique Local Minimizer in the Proxy Segment Cost $F_k(\rho, \theta)$

It can be found that $F_k(\rho, \theta)$ has a unique local minimizer $\rho_k^*(\theta)$ for each θ, justifying the stopping criterion (ii) in Algorithm 1.

First, it can be shown that $\tilde{f}_k(l, \rho, \theta)$ is quasiconvex and $l_k^*(\rho, \theta)$ is a unique local minimizer. Recall that a quasiconvex function $f(x)$ is a function of which the sub-level set $\mathcal{C}_\alpha = \{x : f(x) \leq \alpha\}$ is convex. Moreover, a function $f(x)$ is *strictly* quasiconvex if $f(\lambda x_1 + (1-\lambda)x_2) < \max\{f(x_1), f(x_2)\}$ for any $0 < \lambda < 1$ and $x_1 \neq x_2$. Thus, the following result can be established.

Proposition 2 (Unique Partial Minimizer I): For Type I and Type II cost functions, $\tilde{f}_k(l, \rho, \theta)$ is strictly quasiconvex in l and admits a unique local minimizer $l_k^*(\rho, \theta)$ in $\mathcal{L}(\rho)$, i.e., *$\partial \tilde{f}_k / \partial l < 0$ for $l < l_k^*(\rho, \theta)$ and $\partial \tilde{f} / \partial l > 0$ for $l > l_k^*(\rho, \theta)$.*

Proof: See Appendix A. □

Proposition 2 implies that $l^*(\rho, \theta)$ can be found efficiently using algorithms such as bisection search. The solution can be obtained in $\left\lceil \log_2 \frac{\rho \Delta H}{\epsilon H_{\mathrm{s}}} \right\rceil$ steps, where $\epsilon > 0$ is the error tolerance and $\Delta H = H_{\max} - H_{\min}$.

Proposition 3 (Unique Partial Minimizer II): For Type I and Type II cost functions, the proxy cost function $F_k(\rho, \theta)$ is strictly quasiconvex in ρ, and there is a unique local minimizer $\rho_k^*(\theta)$ of $F_k(\rho, \theta)$, i.e., *$F_k(\rho_1, \theta) > F_k(\rho_2, \theta)$ for $\rho_1 < \rho_2 < \rho_k^*(\theta)$, and $F_k(\rho_3, \theta) < F_k(\rho_4, \theta)$ for $\rho_k^*(\theta) < \rho_3 < \rho_4$.*

Proof: See Appendix B. □

As $F_k(\rho, \theta)$ has a unique local minimum $\rho_k^*(\theta)$ for each θ, there is no need to search in $\rho \geq \rho_k^*(\theta)$, corresponding to the region satisfying $\partial F_k(\rho, \theta)/\partial \rho \geq 0$, which is the stopping criterion (ii) in Algorithm 1.

B. Linear Search Complexity and Quasilinear Computational Complexity

1) Linear Search Complexity: The search complexity is defined as the length of the UAV search path. We first show the following result for the stopping criterion (i) in Algorithm 1.

Proposition 4 (Search Region): The solution $\rho_k^*(\theta)$ that minimizes $F_k(\rho, \theta)$ satisfies $\rho_k^*(\theta) \leq \frac{H_s}{H_{\min}} L \cos\theta$.

Proof: Please refer to Appendix C. □

Then, as a result of Proposition 4, it can be shown that the worst-case search length of Algorithm 1 is a linear function of the radius of the target area.

Theorem 1 (Maximum Trajectory Length): The length of the search trajectory from Algorithm 1 is upper bounded by $(2.4K - 1.4)\frac{H_s}{H_{\min}} L$.

Proof: (Sketch) One can show that the iteration in Step 3 never decreases ρ and θ. On the other hand, the search region is bounded due to Proposition 4. Therefore, the search length is only linear in the scale of the target area. The detail calculation is similar to the case studied in [9, Theorem 2]. □

The sampling complexity is thus upper bounded by $(2.4K-1.4)\frac{H_s}{H_{\min}}L/\delta$, with δ being the step size in Algorithm 1. As a comparison, a naive exhaustive search may require $\mathcal{O}(L^3/\delta)$ search complexity.

2) Quasilinear Computational Complexity: The computational complexity of the proposed algorithm is dominated by the number of evaluations of the proxy segment cost function $F_k(\rho,\theta)$, which involves $\left\lceil \log_2 \frac{\rho\Delta H}{\epsilon H_s} \right\rceil$ evaluations of the original cost function f as previously discussed following Proposition 2. In particular, computing the search direction in (17) involves four evaluations of F_k using the differential formula in (17). Then, it can be shown that the complexity is upper bounded by $(10.6K-9.6)(\log_2 L - \log_2 \epsilon H_s)\frac{L}{\delta}$, which is roughly $\mathcal{O}(KL\log L/\delta)$ in term of the number of evaluations of F_k. Again, a naive exhaustive algorithm may require $\mathcal{O}(L^3/\delta)$ complexity.

C. Global Optimality

Somewhat surprisingly, we can show that, although the search has a linear length, the algorithm can find the globally optimal position in 3D with an arbitrary number of propagation segments.

An intuitive explanation on the global optimality is as follows. First, as a result of the specialized angular coordinate system (l,ρ,θ) developed in Section III-A, the optimal solution $l^*(\rho,\theta)$ given (ρ,θ) can be analytically computed without navigating the UAV to physically search along l. Thus, the 3D spatial search problem degenerates to a 2D one. Second, under some mild conditions on the original cost functions $f_k(x,y)$ in (4), the proxy cost functions $F_k(\rho,\theta)$ in (13) has some nice properties, such as the uniqueness of the local minimizer $\rho_k^*(\theta)$ for each θ, that can be exploited by Algorithm 1. Studying these key features, global optimality in 3D can be established as follows.

Consider a continuous-time algorithm trajectory $\mathbf{x}(t)$, which is obtained from Algorithm 1 using infinitesimal step size $\delta=\kappa dt$ at each infinitesimal time slot dt. Correspondingly, the time series of the minimum cost $F_{\min}(t)$ and $(\hat{\rho}(t),\hat{\theta}(t))$ defined in Algorithm 1 are continuous-time processes.

Theorem 2 (Global Optimality): For Type I and Type II cost functions, the process $(\hat{\rho}(t),\hat{\theta}(t))$ from Algorithm 1 converges to the globally optimal solution (ρ^*,θ^*) to problem $\mathscr{P}''$ in finite time $t=T<\infty$. In addition, the corresponding $\mathbf{x}(l^*(\rho^*,\theta^*),\rho^*,\theta^*)$ obtained from (9) is the globally optimal solution to problem $\mathscr{P}$.

Proof: (Sketch) One can easily establish the following property for given any $\theta'\neq 0$.

$$\min_{\rho\geq 0} F_k(\rho,\theta') \leq \min_{j\geq k} \min_{\substack{\rho\geq 0,\theta\theta'>0 \\ |\theta'|\leq|\theta|\leq\pi/2}} F_j(\rho,\theta). \tag{21}$$

To see this, we note that $F_k(\rho,\theta)=\tilde{f}_k(l^*(\rho,\theta),\rho,\theta)$ from Definition 1 and $\tilde{f}_k(l,\rho,\theta')<\tilde{f}_k(l,\rho,\theta)$ for any $\rho\geq 0$ and $l\in\mathcal{L}(\rho)$, because the UAV-BS distance $d_{\rm b}$ increases when increasing $|\theta|$ (see Equation (25)), but the UAV-user distance $d_{\rm u}=l$ remains unchanged.

As Algorithm 1 is identical to [9, Algorithnm 1], which was developed on the 2D case, except for the construction of $F_k(\rho,\theta)$. We also note from (21) and Propositions 3 and 4 that, the proxy segment cost functions $F_k(\rho,\theta)$ have the same properties as those discussed in [9, Theorem 1]. Therefore, Algorithm 1 finds the globally optimal solution to $\mathscr{P}''$. Due to the equivalence from the angular transformation, the global optimality of the 3D problem $\mathscr{P}$ is thus confirmed. One can follow [9, Appendices C, D] for the details of the proof. □

V. Applications

In this section, we list three example formulations for $\mathscr{P}$. The objective functions of the first two examples respectively match with the Type I and Type II conditions in Section IV-A. The objective of the third example does not match with either of the conditions. We will numerically evaluate the performance of these applications in an actual urban city topology in Section VI.

A. Minimize the Outage Probability

Consider the deployment of a relay network to lower the link outage probability under a certain end-to-end target data rate. The UAV relay operates in an amplify-and-forward (AF) mode, where it simply redirects the signal from the BS to the user by amplifying the signal. Specifically, denote the received signal at the UAV relay as $y_{\rm r}=\sqrt{P_{\rm b}g_{\rm r,b}}a_{\rm r,b}s+n_{\rm r}$, where $P_{\rm b}$ is the transmit power at the BS, $g_{\rm r,b}$ is the large scale fading including the path loss and shadowing of the BS-UAV link, $a_{\rm r,b}$ is a random variable to model the small scale fading, and $s,n_{\rm r}\sim\mathcal{CN}(0,1)$ models the transmit signal and receive noise, respectively.

Under the AF mode, the relay signal is given by $s_{\rm r}=y_{\rm r}/\sqrt{P_{\rm b}g_{\rm r,b}|a_{\rm r,b}|^2+1}$ where the denominator is a scaling factor to normalize the transmission power at the UAV. The receive signal at the user is thus given by $y_{\rm u}=\sqrt{P_{\rm r}g_{\rm u,r}}a_{\rm u,r}s_{\rm r}+n_{\rm u}$, where $P_{\rm r}$ is the transmit power at the UAV, $g_{\rm u,r}$ and $a_{\rm u,r}$ are the large scale fading variable and small scale fading variable of the UAV-user link, respectively. Finally, $n_{\rm u}\sim\mathcal{CN}(0,1)$ is the receive noise. We assume that $|a_{\rm r,b}|^2$ and $|a_{\rm u,r}|^2$ follow exponential distribution with parameter $\lambda=1$, a common assumption of Rayleigh fading channels.

The relay channel capacity is given by $C_{\rm AF}=\frac{1}{2}\log_2(1+q(P_{\rm b}g_{\rm r,b}|a_{\rm r,b}|^2,P_{\rm r}g_{\rm u,r}|a_{\rm u,r}|^2))$, where $q(x,y)\triangleq xy((x+y+1)$ and the constant $\frac{1}{2}$ is to capture the fact that the signal requires two time slots to reach the user [31], [32]. The outage probability w.r.t. a target data rate R can be shown to be $\mathbb{P}\{C_{\rm AF}<R\}\approx(\frac{1}{P_{\rm b}g_{\rm r,b}}+\frac{1}{P_{\rm r}g_{\rm u,r}})(2^{2R}-1)^2$ under high SNR, *i.e.*, $P_{\rm b}g_{\rm r,b},P_{\rm r}g_{\rm u,r}\gg 1$ [32, Lemma 1].

To minimize the outage probability $\mathbb{P}\{C_{\rm AF}<R\}$ for the large-scale propagation statistics and LOS conditions, one can formulate problem $\mathscr{P}$ by choosing

$$f_k(d_{\rm u},d_{\rm b})=\frac{1}{P_{\rm b}\beta_0 d_{\rm b}^{-\alpha_0}}+\frac{1}{P_{\rm r}\beta_k d_{\rm u}^{-\alpha_k}},\quad k=1,2,\ldots,K \tag{22}$$

where β_k is approximately $10^{b_k/10}$ and $\alpha_k = a_k/10$ for a_k, b_k given in (2). One can verify that the objective function f_k satisfies the Type I condition. Hence, from Theorem 2, Algorithm 1 will find the globally optimal UAV position in 3D space.

B. Maximize the Capacity

Consider a decode-and-forward (DF) relay system where the UAV servers as a relay. The relay channel capacity of such a DF system can be shown to be $C_{\text{DF}} = \frac{1}{2}\min\{\log_2(1+P_{\text{b}}g_{\text{r,b}}|a_{\text{r,b}}|^2), \log_2(1+P_{\text{r}}g_{\text{u,r}}|a_{\text{u,r}}|^2)\}$ [32], [33]. In an actual system, the averaged achievable data rate will depend on the average SNR $P_{\text{b}}g_{\text{r,b}}$ and $P_{\text{r}}g_{\text{u,r}}$ through a number of factors such as channel fading, channel coding schemes, modulation schemes, and rate adaptation strategy. As discussed in [34], this process can be abstracted using a discount factor κ, $0 < \kappa < 1$, resulting in a simplified, but widely-used model for the effective SNR. Then, the relay capacity is given by $C_{\text{DF}} = \frac{1}{2}\min\{\log_2(1+\kappa P_{\text{b}}g_{\text{r,b}}), \log_2(1+\kappa P_{\text{r}}g_{\text{u,r}}), r_{\max}\}$. Based on the analysis in [34], a typical choice of κ is $\kappa = 0.5$.

To maximize the relay channel capacity, one populates problem $\mathscr{P}$ by choosing

$$f_k(d_{\text{u}}, d_{\text{b}}) = \frac{1}{2}\min\{\log_2(1+\kappa P_{\text{b}}\beta_0 d_{\text{b}}^{-\alpha_0}), \log_2(1+\kappa P_{\text{r}}\beta_k d_{\text{u}}^{-\alpha_k}), r_{\max}\} \quad (23)$$

for $k = 1, 2, \ldots, K$, with $\beta_k = 10^{b_k/10}$ and $\alpha_k = a_k/10$ according to (2).

One can verify that the objective function f_k satisfies the Type II condition. Hence, from Theorem 2, Algorithm 1 will find the globally optimal UAV position in 3D space.

Note that our formulation (23) ignores the residual shadowing ξ_k in (2), and hence, the optimal solution to $\mathscr{P}$ only results in a sub-optimal solution in practice. Nevertheless, the numerical study in Section VI-E shows that, compared to the baseline, the performance obtained from optimizing (23) is already quite close to a genie-aided one that takes into account the residual shadowing ξ_k and requires exhaustive search in 3D.

C. Energy Minimization for Data Collection

Suppose that the UAV needs to navigate to a remote location and deliver B message bits to a user using a DF relay strategy. We assume that the UAB-BS link is strong enough, and hence, the end-to-end capacity is given by the capacity of the UAV-user link $r_{\text{u}}(d_{\text{u}}) = \frac{1}{2}\min\{\log_2(1+\kappa P_{\text{r}}g_{\text{u,r}}(d)), r_{\max}\}$. To further simplify the problem, we assume that the UAV only transmits when it reaches the desired position.[2] A related problem with similar arguments was also studied in [8] under a more complex multi-hop scenario, but we want to keep the example simple here for clarity. The required transmission time is $t_{\text{tx}} = B/(Wr_{\text{u}}(d))$, where W is the bandwidth.

Denote P_{cruise}, P_{hover}, and P_{circuit}, as the UAV cruise power, the UAV hover power, and the circuit power for data processing, respectively. Note that, in reality, the power consumption may depend on various factors such as the UAV speed. If we focus on the operation under a constant UAV speed, then the cruise power P_{cruise} is roughly constant. Thus, the power consumed at the navigation phase is $P_{\text{cruise}}d/v$ and the energy consumed at the transmission phase is $(P_{\text{hover}} + P_{\text{circuit}} + P_{\text{r}})B/(Wr_{\text{u}}(d))$, where d is the distance from the initial UAV position and v is the speed.[3] Therefore, the total energy consumed to deliver the total B bits is given by $E = P_{\text{cruise}}\frac{d}{v} + \frac{(P_{\text{hover}}+P_{\text{circuit}}+P_{\text{r}})B}{Wr_{\text{u}}(d)}$.

To optimize for the large-scale propagation characteristics and LOS conditions, the target UAV position that minimizes the total energy consumption E can be found by solving problem $\mathscr{P}$, where the objective function can be chosen as, for $k = 1, 2, \ldots, K$,

$$f_k(d_{\text{u}}, d) = P_{\text{cruise}}\frac{d}{v} + \frac{(P_{\text{hover}} + P_{\text{circuit}} + P_{\text{r}})B}{\frac{1}{2}W \cdot \min\{\log_2(1+\kappa P_{\text{r}}\beta_k d_{\text{u}}^{-\alpha_k}), r_{\max}\}}.$$

One can verify that f_k is increasing in both d_{u} and d, respectively. However, f_k does not satisfy either Type I or Type II conditions. Therefore, the global optimality of Algorithm 1 for such an energy minimization problem is still unclear. However, as will be observed from the numerical experiments in Section VI-F, the performance between Algorithm 1 and that of an exhaustive search is nearly indistinguishable.

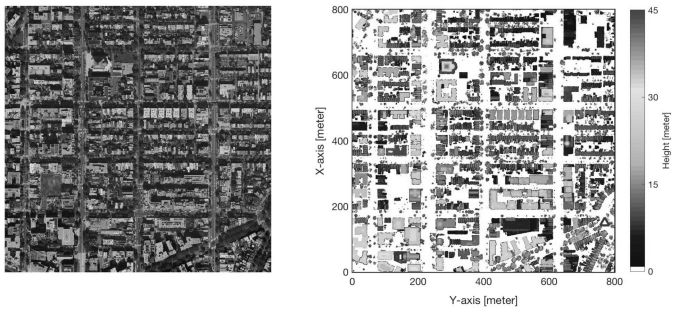

Fig. 4. (Left) An orthoimagery of an 800 [m] × 800 [m] area in Washington DC, USA. (Right) The corresponding elevation map of buildings and vegetation. The BS is placed at the red triangle with 45 meter height.

VI. Numerical Results

A. Propagation Environment Modeling

We study the city environment using the geographical data captured in central Washington DC, USA in 2013.[4] Fig. 4 shows the orthoimagery of an 800 m × 800 m area of interest and the corresponding elevation map. In this area, the maximum building height is 45 meters. Building areas are designated by black polygons, whereas, the colored pixels outside the building areas represent the urban vegetation. The BS antenna is placed at 45 meter height. For each experiment

[2]We also observe from numerical experiments that the UAV is mostly in deep shadowing during its course to the target position. In this case, the transmission during the UAV navigation phase is negligible.

[3]We assume that the UAV consumes the same power P_{cruise} regardless of its direction of mobility. Such an approximation is motivated from the experiment results in [35], where there is only 10% power difference between the UAV ascending and UAV hovering.

[4]The original data was obtained from the USGS database: http://ngmdb.usgs.gov. The processed dataset is available at IEEE DataPort with DOI: 10.21227/y6gg-j788.

TABLE II
DEFAULT NETWORK PARAMETERS

Parameter	Description
BS	Located at (150, 770, 45) in Fig. 4 (red triangle)
User	Uniformly dropped at the ground level in the non-building area
Carrier frequency	2.5 GHz (3GPP), 28 GHz (mmW)
Bandwidth	20 MHz (3GPP), 500 MHz (mmW)
Transmit power	33 dBm (BS), 30 dBm (UAV)
Noise figure	7 dB
Antenna (3GPP)	Single antenna
Antenna (mmW)	4×4 half-wavelength uniform planar array with 20 dB beamforming gain
Path loss (LOS)	3GPP: $22.0 + 28.0 \log_{10}(d) + 20 \log_{10} f_c$, mmW: $61.4 + 20.0 \log_{10}(d)$, $\sigma_{\text{SF}} = 1$ dB
Path loss (OLOS)	3GPP: $32.0 + 28.0 \log_{10}(d) + 20 \log_{10} f_c$, mmW: $81.4 + 20.0 \log_{10}(d)$, $\sigma_{\text{SF}} = 3$ dB
Path loss (NLOS)	3GPP: $22.7 + 36.7 \log_{10}(d) + 26 \log_{10} f_c$, mmW: $72.0 + 29.2 \log_{10}(d)$, $\sigma_{\text{SF}} = 5$ dB
UAV power	200 W (cruise), 200 W (hover), 2 W (circuit)
UAV configuration	Speed: 5 m/s, Minimum height: 45 m, Maximum height: 120 m

below, we evaluate 10,000 uniformly random user locations in the non-building area. The minimum UAV height is set to 45 meters to avoid collision with any building while maintaining LOS condition with the BS; the maximum height is 120 meters to obey the US regulation.

We employ a ray-tracing method to identify three propagation conditions: LOS, if there is no building or vegetation blocking the direct ray from the transmitter to the receiver, OLOS, if there is only vegetation blockage of the direct ray, and NLOS, if there is a building that blocks the direct ray. Corresponding path loss models and shadowing parameters σ_{SF} are used as specified in Table II. The residual shadowing is modeled as $\mathcal{N}(0, \sigma^2_{\text{SF}})$.

B. Air Interface

We evaluate two air interfaces. One transmits at 2.5 GHz with propagation parameters taken from the 3GPP Urban Micro (UMi) model in [36]. The other transmits at 28 GHz with parameters taken from the experiment results reported in [37]. Since both the standard cellular model [36] and the experiment in [37] consider only two propagation scenarios, LOS and NLOS, we simulate the parameter for the OLOS condition by adding 10 dB (3GPP case), or 20 dB (mmW case), vegetation penetration loss from the LOS models in [36] and [37], respectively.

For millimeter wave (mmW) links, we assume half-wavelength 4×4 uniform planar arrays at the BS transmitter, UAV transceiver, and the user receiver. The beamforming is computed using channel statistics. Experimental results in [37] showed that a 9–12 dB gain under long-term beamforming can usually be achieved at the user side. Therefore, we assume a 20 dB beamforming gain combined from both the transmitter and receiver. The key parameters are summarized in Table II.

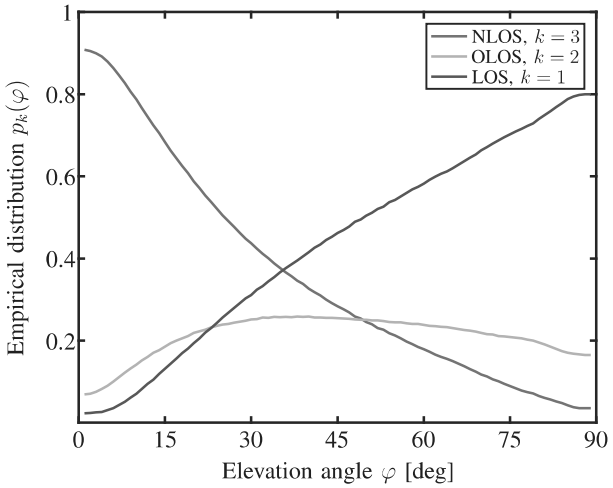

Fig. 5. Statistics of propagation conditions.

C. Baseline Schemes and Observations

We evaluate the UAV placement method in Algorithm 1 with step size $\delta = 3$ meters; we compare performance with the following four baseline schemes:

- *Direct BS-user link:* The scheme transmits at the direct BS-user link, without the help of the UAV relay. In the urban topology depicted in Fig. 4, we numerically found that there are only 3.3% users in LOS condition to the BS and less than 20% users in OLOS condition. The LOS ratio at the 89 degree elevation angle corresponds to the fact that roughly 20% of the street is covered by vegetation as shown in Fig. 4.
- *Statistical Method:* Define $p_k(\varphi(\mathbf{x})) = \mathbb{P}\{\mathbf{x} \in \mathcal{D}_k | \varphi\}$ as the conditional probability of the UAV position $\mathbf{x}$ belonging to the kth propagation segment given the elevation angle φ from the user to the UAV. The empirical distributions $p_k(\varphi)$ are obtained in an offline mode from a large amount of channel measurement data over various user and UAV positions in Fig. 4. The results are plotted in Fig. 5. Given $p_k(\varphi)$, the UAV position is obtained by solving

$$\mathscr{P}'_{\text{stat}}: \underset{\mathbf{x} \in \mathbb{R}^3}{\text{minimize}} \quad \sum_{k=1}^{K} f_k(d_{\text{u}}, d_{\text{b}}) p_k(\varphi(\mathbf{x}))$$
$$\text{subject to } H_{\min} \le x_3 \le H_{\max}$$

  using an exhaustive search algorithm. Note that under $K = 2$, this method is conceptually identical to the probabilistic LOS method in the literature [14], [15].
- *1D Exhaustive Search:* This schemes performs an exhaustive search along the BS-user axis on the $x_3 = H_{\min}$ plane and finds the UAV position that minimizes the objective function of $\mathscr{P}$. The UAV relays then relays the message to the user, while the direct BS-user link is completely ignored.
- *3D Exhaustive Search:* This schemes performs an exhaustive search over a 3D lattice with 3 meter spacing. The lattice that achieves the minimum cost in $\mathscr{P}$ is chosen as the optimal UAV position.

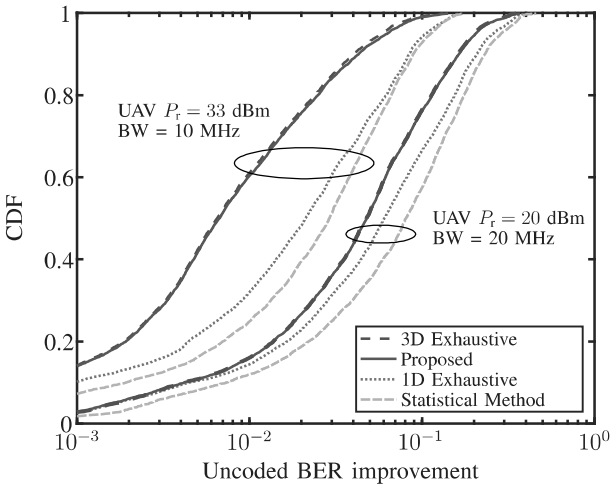

Fig. 6. Outage probability.

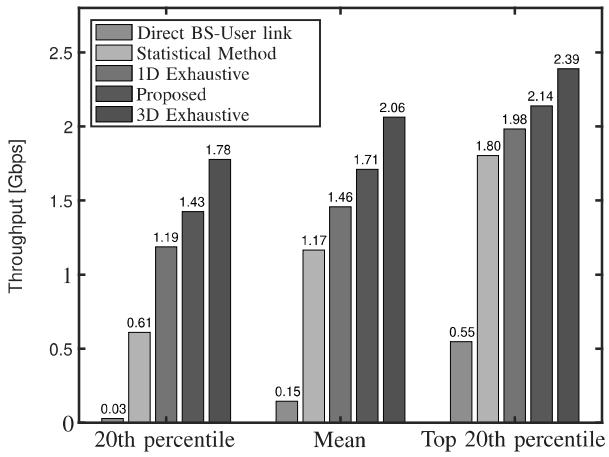

Fig. 7. Throughput evaluation over 10,000 user positions under the presence of shadowing.

D. Outage Probability Minimization and the Confirmation on the Global Optimality

Consider the outage probability minimization problem in Section V-A. The performance is evaluated using the 3GPP Urban Micro (UMi) model and the residual shadowing is ignored as discussed in Section V-A. We normalize the outage probability in (22) from various UAV schemes by the outage probability of the direct BS-user link for each user. Note that the ratio is equivalent to the uncoded bit error rate (BER) improvement, and the cumulative distribution functions (CDFs) of the improvement are plotted in Fig. 6. Two cases are evaluated using the default parameters in Table II except for those specified in the figure.

It is observed that the proposed scheme can substantially reduce the uncoded BER over the statistical scheme. In particular, when the UAV-to-user link is stronger, the proposed scheme can achieve much more reduction from the statistical scheme. This is because the proposed scheme finds a position closer to the BS while still maintaining a good propagation condition (such as LOS) to the user. In addition, it is observed that the CDF curves of the proposed scheme coincide with those from the exhaustive search, numerically confirming that the proposed algorithm finds the globally optimal solution to $\mathscr{P}$.

E. Capacity Maximization

Consider a system that operates in a hybrid transmission mode with an objective to maximize the capacity in Section V-B. Specifically, if the propagation condition is in LOS or OLOS, the mmW radio interface at 28 GHz is used for transmission; otherwise, the 3GPP radio interface at 2.5 GHz is used. The shadowing parameters are specified in Table II. The algorithm optimizes $\mathscr{P}$ in (4) with the cost functions specified in (23).

1) Robustness Under Shadowing: Note that the formulation in (23) ignores the shadowing when searching for the best UAV position, while the performance is evaluated under the presence of shadowing as specified in Table II. In other words,

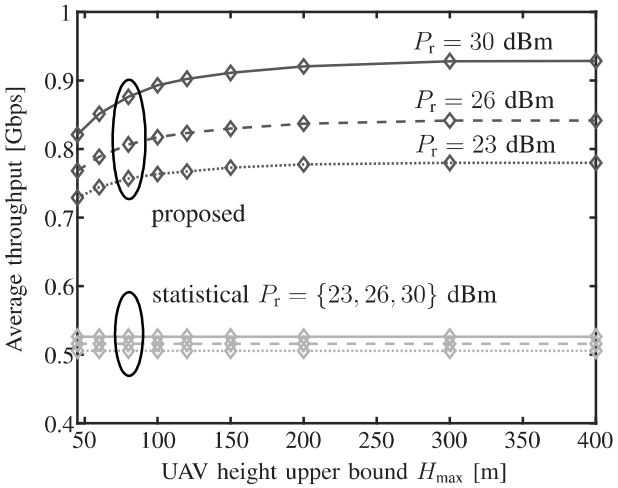

Fig. 8. Average throughput under various maximum permissible UAV height $H_{\max}$.

the globally optimal solution to $\mathscr{P}$ is not necessarily the position that achieves the maximum throughout under the presence of shadowing. In this experiment, we observe 17% performance degradation from exhaustive search in terms of average throughput as shown in Fig. 7.

As observed, even when the model assumptions are violated, the proposed algorithm still yields good performance. First, it is observed that the proposed scheme achieves more than 80% throughput of the 3D exhaustive scheme for all categories in Fig. 7. Note that the proposed scheme only requires a spatial search path that is linear in the diameter of the target area, but an exhaustive search would require a cubic path. By contrast, the statistical method perform substantially worse. Second, for the users in deep shadow (the 20th percentile), the proposed scheme can deliver over 2X throughput of that from the statistical method.

2) Impact on the Maximum UAV Height $H_{\max}$: Fig. 8 demonstrates the average throughput versus the maximum permissible UAV height $H_{\max}$ under 23 dBm BS transmission power and various UAV transmission power. First, we find

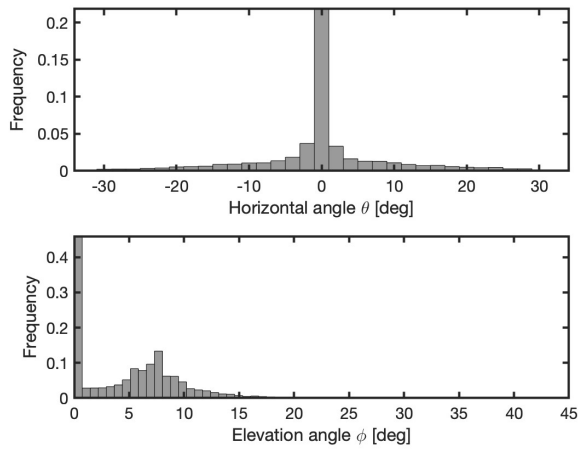

Fig. 9. Histograms of the optimal UAV positions in deviation angle and elevation angle w.r.t. the BS-user direction.

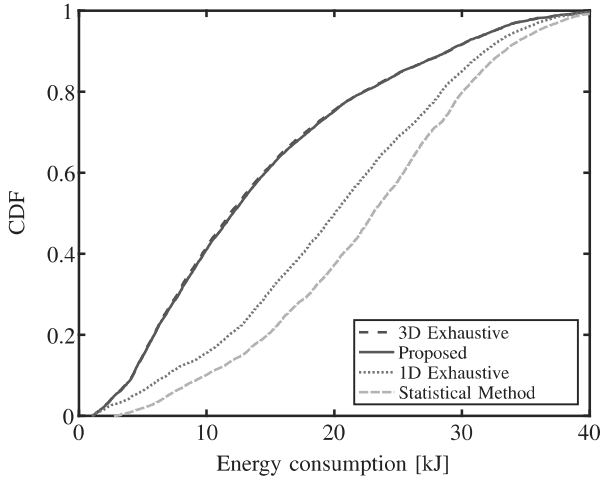

Fig. 10. Distribution of the energy consumption.

TABLE III
AVERAGE LENGTH OF THE SPATIAL SEARCH TRAJECTORY

1D Search	**Proposed**		**2D Exhaustive**
	$H_{\rm s} = 50$ **m**	$H_{\rm s} = 120$ **m**	
459 m	614 m	706 m	83.4 km

that the larger $H_{\max}$, the higher the average throughput. This confirms the advantage of the 3D optimization for UAV relay position. Second, it is also found that the larger the UAV power, the more gain to be achieved by increasing $H_{\max}$. Finally, for the statistical method baseline, it does not benefit from adjusting the UAV height, because its optimal solution is always attained at the minimum UAV height from our experiment.

3) Statistics on the Optimal UAV Position in 3D: Fig. 9 shows the histograms of the optimal UAV positions in terms of the deviation angle θ and elevation angle ϕ w.r.t. to the BS-user direction. It is observed that the optimal UAV positions tend to have small deviation angle and elevation angle. Such a property may provide insights in designing approximate solutions to handle the practical issue of non-isotropic antenna pattern at the BS.

4) Length of the Spatial Search Trajectory: Table III summarizes the average length of the spatial search trajectory for each scheme over 10,000 user locations. Note that performance bottleneck is the physical length of the search path that UAV explores over. As observed, the path lengths of the proposed scheme under different search parameters $H_{\rm s}$ (see Algorithm 1) are comparable to that of the 1D Exhaustive Search baseline, numerically confirming Theorem 1, which states that the search path has linear length in the diameter of the target area.

F. Energy Minimization

For the energy minimization problem in Section V-C, we also consider the hybrid transmission model discussed in Section VI-E. The UAV is required to deliver $B = 10$ Giga bits to a user which may be in deep shadow at its BS-user link.

Fig. 10 plots the distribution of the total energy consumption for different schemes. It is observed that the proposed UAV placement algorithm can reduce the total energy consumption by a half from a statistical method. Moreover, the proposed scheme significantly outperforms the 1D Exhaustive Search method. This suggests that the optimal UAV position usually *not* lies on the BS-user axis. Finally, the performance of the proposed scheme matches with that from the exhaustive search, which implies that the proposed Algorithm 1 still finds the globally optimal UAV position in this special example, despite violating the conditions in Theorem 2.

VII. CONCLUSION

This paper developed an efficient search algorithm to find the globally optimal UAV position for establishing the best relay link between a BS and a user. A key problem addressed here was to avoid signal blockage for the UAV-to-user link. As oppose to statistical methods, the proposed algorithm measures the LOS condition on the fly and adapts to the local propagation environment. The worst case search length was shown to be bounded by a linear function of the BS-user distance. In addition, the algorithm has been proven to find the globally optimal UAV position in 3D for several types of cost functions. The results were further confirmed by numerical experiments over a real terrain topology, where the proposed method significantly outperformed the method based on stochastic terrain models.

APPENDIX A
PROOF OF PROPOSITION 2

A. Proof for Type I Functions

Define the squared distances as $D_{\rm b} = d_{\rm b}^2$ and $D_{\rm u} = d_{\rm u}^2$ for simple notation. From the geometric relations between the three positions $\mathbf{x}$, $\mathbf{x}_{\rm b}$, and $\mathbf{x}_{\rm u}$, and recall that $L \triangleq \|\bar{\mathbf{x}}_{\rm u} - \bar{\mathbf{x}}_{\rm b}\|_2$,

we have

$$D_{\mathrm{u}}(l) = l^2 \tag{24}$$

$$D_{\mathrm{b}}(l,\rho,\theta) = L^2\sin^2\theta + \Big(L\cos\theta - \frac{\rho l}{\sqrt{\rho^2+H_{\mathrm{s}}^2}}\Big)^2 + \Big(\frac{lH_{\mathrm{s}}}{\sqrt{\rho^2+H_{\mathrm{s}}^2}} - H_{\mathrm{b}}\Big)^2 \tag{25}$$

Lemma 1: Suppose that the functions $D_u(\mathbf{z})$ and $D_b(\mathbf{z})$ are strictly convex in $\mathbf{z}$. Then, for Type I function $f_k(x,y)$, the composite function $f_k(D_u^{1/2}, D_b^{1/2})(\mathbf{z})$ is strictly convex in $\mathbf{z}$.

Proof: From the chain rule and the fact that $d_{\mathrm{u}} = D_{\mathrm{u}}^{1/2}$ and that $f_k(x,y)$ is non-decreasing in x and y, we have $\frac{\partial f_k}{\partial D_{\mathrm{u}}} = \frac{\partial f_k}{\partial d_{\mathrm{u}}}\frac{\partial d_{\mathrm{u}}}{\partial D_{\mathrm{u}}} = \frac{\partial f_k}{\partial d_{\mathrm{u}}}\frac{1}{2\sqrt{D_{\mathrm{u}}}} > 0$. The second order derivative is then given by

$$\begin{aligned}\frac{\partial^2 f_k}{\partial D_{\mathrm{u}}^2} &= \frac{\partial}{\partial D_{\mathrm{u}}}\Big(\frac{\partial f_k}{\partial d_{\mathrm{u}}}\frac{1}{2\sqrt{D_{\mathrm{u}}}}\Big)\\ &= \frac{\partial^2 f_k}{\partial d_{\mathrm{u}}^2}\Big(\frac{\partial d_{\mathrm{u}}}{\partial D_{\mathrm{u}}}\Big)\frac{1}{2\sqrt{D_{\mathrm{u}}}} + \frac{\partial f_k}{\partial d_{\mathrm{u}}}\frac{\partial}{\partial D_{\mathrm{u}}}\Big(\frac{1}{2\sqrt{D_{\mathrm{u}}}}\Big)\\ &= \frac{1}{4d_{\mathrm{u}}^2}\Big(\frac{\partial^2 f_k}{\partial d_{\mathrm{u}}^2} - \frac{\partial f_k}{\partial d_{\mathrm{u}}}\frac{1}{d_{\mathrm{u}}}\Big) \geq 0\end{aligned}$$

where the last inequality is from condition (18).

Similarly, we can obtain $\frac{\partial f_k}{\partial D_{\mathrm{b}}} > 0$ and $\frac{\partial^2 f_k}{\partial D_{\mathrm{b}}^2} \geq 0$.

Define an operator ∇ as $\nabla \triangleq [\frac{\partial}{\partial z_1}\ \frac{\partial}{\partial z_2}\ \dots\ \frac{\partial}{\partial z_M}]^{\mathrm{T}}$, where z_m is the mth entry of $\mathbf{z}$. We have $\nabla f_k = \frac{\partial f_k}{\partial D_{\mathrm{u}}}\nabla D_{\mathrm{u}} + \frac{\partial f_k}{\partial D_{\mathrm{b}}}\nabla D_{\mathrm{b}}$. In addition, noticing that $\frac{\partial^2 f_k}{\partial d_{\mathrm{u}}\partial d_{\mathrm{b}}} = 0$, we arrive at

$$\nabla^2 f_k = \frac{\partial^2 f_k}{\partial D_{\mathrm{u}}^2}\nabla D_{\mathrm{u}}\nabla D_{\mathrm{u}}^{\mathrm{T}} + \frac{\partial f}{\partial D_{\mathrm{u}}}\nabla^2 D_{\mathrm{u}} + \frac{\partial^2 f}{\partial D_{\mathrm{b}}^2}\nabla D_{\mathrm{b}}\nabla D_{\mathrm{b}}^{\mathrm{T}} + \frac{\partial f}{\partial D_{\mathrm{b}}}\nabla^2 D_{\mathrm{b}} \succeq \mathbf{0}$$

which shows that $f_k(D_{\mathrm{u}}^{1/2}, D_{\mathrm{b}}^{1/2})(\mathbf{z})$ is convex in $\mathbf{z}$. In addition, since $D_{\mathrm{u}}(\mathbf{z})$ and $D_{\mathrm{b}}(\mathbf{z})$ are *strictly* convex in $\mathbf{z}$, we then conclude that $f_k(D_{\mathrm{u}}^{1/2}, D_{\mathrm{b}}^{1/2})(\mathbf{z})$ is *strictly* convex in $\mathbf{z}$. □

From (24)–(25), we know that $D_{\mathrm{u}}(l,\rho,\theta)$ and $D_{\mathrm{b}}(l)$ are strictly convex in l. Then, using Lemma 1, we can conclude that $f_k(d_{\mathrm{u}}, d_{\mathrm{b}})(l,\rho,\theta)$ is strictly convex in l, and hence, $\tilde{f}_k(l,\rho,\theta)$ admits a unique local minimum at $l_k^*(\rho,\theta)$ over the interval $\mathcal{L}(\rho)$, which is convex and compact. Since it is strictly convex, $\tilde{f}_k(l,\rho,\theta)$ is also strictly quasiconvex.

B. Proof for Type II Functions

Exploiting the increasing functions $f^{(1)}(x)$ and $f^{(2)}(y)$, we define $\tilde{f}_k^{(1)}(l) \triangleq f_k^{(1)}(D_{\mathrm{u}}^{1/2})(l)$ and $\tilde{f}_k^{(2)}(l,\rho,\theta) \triangleq f_k^{(2)}(D_{\mathrm{b}}^{1/2})(l,\rho,\theta)$. Condition (20) implies that

$$\tilde{f}_k(l,\rho,\theta) = \max\{\tilde{f}_k^{(1)}(l), \tilde{f}_k^{(2)}(l,\rho,\theta)\}. \tag{26}$$

Lemma 2: Let $f_1(x)$ and $f_2(x)$ be positive and strictly increasing functions. In addition, let $g_1(\mathbf{y})$ and $g_2(\mathbf{y})$ be strictly convex functions. Then, the composite function $f(\mathbf{y}) = \max\{f_1(g_1)(\mathbf{y}),\ f_2(g_2)(\mathbf{y})\}$ is strictly quasiconvex in $\mathbf{y}$.

Proof: Suppose that $\mathbf{y}_1, \mathbf{y}_2 \in \mathcal{C}_\alpha = \{\mathbf{y} : f(\mathbf{y}) \leq \alpha\}$. Let $\max\{f(\mathbf{y}_1), f(\mathbf{y}_2)\} = \alpha_1 \leq \alpha$. Then, $g_i(\mathbf{y}_j) \leq f_i^{-1}(\alpha_1)$ for both $i,j \in \{1,2\}$, by the strictly increasing property of f_i, where $x = f_i^{-1}(y)$ denotes the inverse function of $y = f_i(x)$. From the strict convexity of g_i, we have

$$\begin{aligned} g_i(\lambda\mathbf{y}_1 + (1-\lambda)\mathbf{y}_2) &< \lambda g_i(\mathbf{y}_1) + (1-\lambda)g_i(\mathbf{y}_2)\\ &\leq \lambda f_i^{-1}(\alpha_1) + (1-\lambda)f_i^{-1}(\alpha_1)\\ &= f_i^{-1}(\alpha_1)\end{aligned}$$

for both $i \in \{1,2\}$ and $\lambda \in (0,1)$. Therefore, $f_i(g_i)(\lambda\mathbf{y}_1 + (1-\lambda)\mathbf{y}_2) < \alpha_1$, and hence $f(\lambda\mathbf{y}_1 + (1-\lambda)\mathbf{y}_2) < \alpha_1 = \max\{f(\mathbf{y}_1), f(\mathbf{y}_2)\}$. This concludes that $f(\mathbf{y})$ is strictly quasiconvex. □

Using Lemma 2, $\tilde{f}_k(l,\rho,\theta)$ in (26) is strictly quasiconvex in l. We then have the following result on the optimality.

Lemma 3 (Optimality From Quasiconvexity): If $f(x)$ is strictly quasiconvex in a convex and closed interval $I \in \mathbb{R}$, then $f(x)$ admits a unique local minimum in I.

Proof: We develop the proof from contradiction. Suppose that $x_0 \in I$ is a global minimizer of $f(x)$, and x_1 is a local minimizer, where $x_1 \neq x_0$. As a result, $f(x_0) < f(x_1)$. without loss of generality (w.l.o.g.), assume that $x_0 < x_1$. Choose an arbitrarily small $\epsilon > 0$, such that $x_2 = x_1 - \epsilon$ is sufficiently close to the local minimizer x_1 and $f(x_2) > f(x_1)$. As a consequence, there exists a $0 < \lambda < 1$, such that $x_2 = \lambda x_0 + (1-\lambda)x_1$. However, according to the quasiconvexity of $f(x)$, it holds that $f(x_2) \leq \max\{f(x_0), f(x_1)\} = f(x_1)$, which violates the fact that x_1 is a local minimum. By contradiction, the local minimum is unique. □

Using Lemma 3, one can conclude that $\tilde{f}_k(l,\rho,\theta)$ admits a unique local minimum $l_k^*(\rho,\theta)$ over $\mathcal{L}(\rho)$.

APPENDIX B
PROOF OF PROPOSITION 3

We exploit a third coordinate system to develop the results. Consider a θ-plane, defined as the 2D plane that is perpendicular to the ground and passing through both the user position $\mathbf{x}_{\mathrm{u}}$ and the UAV position $\mathbf{x}(l,\rho,\theta)$ as illustrated in Fig. 11. Each point $\mathbf{x}(l,\rho,\theta)$ on the θ-plane can be represented by coordinates (y,z) as follows

$$\begin{bmatrix} y \\ z \end{bmatrix} = \mathbf{G}_\theta(l,\rho) = \begin{bmatrix} l\dfrac{\rho}{\sqrt{\rho^2+H_s^2}} \\ l\dfrac{H_s}{\sqrt{\rho^2+H_s^2}} \end{bmatrix} \tag{27}$$

where the mapping $\mathbf{G}_\theta$ is invertible and the reverse transformed is denoted as $(l,\rho) = \mathbf{G}_\theta^{-1}(y,z)$.

On the θ-plane, the squared distances can derived as $D_{\mathrm{b}}^\theta(y,z) = L^2\sin^2\theta + (L\cos\theta - y)^2 + (z - H_{\mathrm{b}})^2$ and $D_{\mathrm{u}}^\theta(y,z) = y^2 + z^2$, which are strictly convex in (y,z). Define the transformed cost function (on the θ-plane) as

$$f_k^\theta(y,z) \triangleq f_k((D_{\mathrm{u}}^\theta)^{1/2}, (D_{\mathrm{b}}^\theta)^{1/2})(y,z). \tag{28}$$

It turns out that f_k^θ is strictly quasiconvex in (y,z) for both Type I and Type II functions. To see this for Type I functions, applying Lemma 1, $f_k^\theta(y,z)$ is shown to be strictly convex in (y,z). Hence, $f_k^\theta(y,z)$ is also strictly quasiconvex in (y,z). For Type II cost functions, we have

$$f_k^\theta(y,z) = \max\{f_k^{(1)}((D_{\mathrm{u}}^\theta)^{1/2})(y,z), f_k^{(2)}((D_{\mathrm{b}}^\theta)^{1/2})(y,z)\}.$$

Using Lemma 2, $f_k^\theta(y,z)$ is strictly quasiconvex in (y,z).

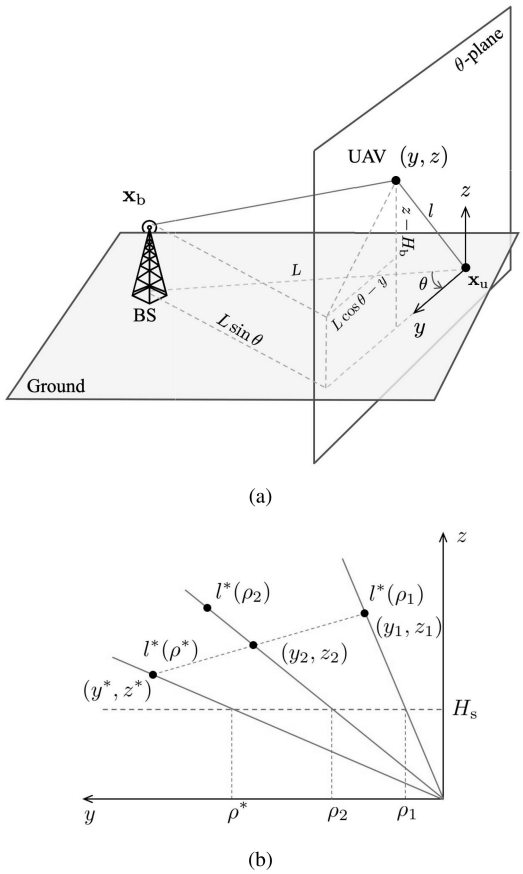

Fig. 11. Geometric interpretation of the θ-plane.

We now study the monotonicity of $F_k(\rho, \theta)$ on the interval $(0, \rho^*)$, where $\rho^*(\theta)$ is the minimizer of $F_k(\rho, \theta)$. Consider an arbitrary ρ_1, such that $0 < \rho_1 < \rho^*$. Denote the coordinates on the θ-plane $(y^*, z^*) = \mathbf{G}_\theta(l_k^*(\rho^*, \theta), \rho^*)$ and $(y_1, z_1) = \mathbf{G}_\theta(l_k^*(\rho_1, \theta), \rho_1)$, where $l_k^*(\rho_1, \theta)$ is the solution to $\mathscr{P}_k'$ given (ρ_1, θ). Note that $f_k^\theta(y^*, z^*) \le f_k^\theta(y_1, z_1)$, since $\rho^*(\theta)$ minimizes $F_k(\rho, \theta)$.

In addition, for some $0 < t < 1$, let $y_2 = ty^* + (1-t)y_1$ and $z_2 = tz^* + (1-t)z_1$. In particular, we choose an arbitrary ρ_2 satisfying $\rho_1 < \rho_2 < \rho^*$, and we choose the parameter $t = \frac{\rho_2 z_1 - H_\mathrm{s} y_1}{\rho_2(z_1 - z^*) + H_\mathrm{s}(y^* - y_1)}$, so that $\mathbf{G}_\theta^{-1}(y_2, z_2) = (l_2, \rho_2)$ for some l_2. Note that $l_2 \in \mathcal{L}(\rho_2)$, because the constraint $H_\min \le x_3 \le H_\max$ in $\mathscr{P}$ is equivalent to $H_\min \le z \le H_\max$ in the θ-plane, and $\rho \ge 0$ is equivalent to $y \ge 0$, which imply that the feasible domain is convex on the θ-plane.

Using these notations, we have

$$\begin{aligned} f_k^\theta(y_2, z_2) &= f_k^\theta(ty^* + (1-t)y_1, tz^* + (1-t)z_1) \\ &< \max\{f_k^\theta(y^*, z^*), f_k^\theta(y_1, z_1)\} \\ &= f_k^\theta(y_1, z_1) \end{aligned}$$

where the inequality comes from the strict quasiconvex of f_k^θ.

As a result, we have

$$\begin{aligned} F_k(\rho_2, \theta) &= f_k(d_\mathrm{u}, d_\mathrm{b})(\mathbf{x}(l_k^*(\rho_2, \theta), \rho_2, \theta)) \\ &\le f_k^\theta(y_2, z_2) < f_k^\theta(y_1, z_1) \end{aligned}$$

where the right hand side satisfies

$$f_k^\theta(y_1, z_1) = f_k(d_\mathrm{u}, d_\mathrm{b})(\mathbf{x}(l_k^*(\rho_1, \theta), \rho_1, \theta)) = F_k(\rho_1, \theta)$$

which concludes the monotonicity of $F_k(\rho, \theta)$ over $(0, \rho^*)$ as ρ_1 and ρ_2 have been chosen arbitrarily.

Similarly, we can show that $F_k(\rho_4, \theta) > F_k(\rho_3, \theta) > F_k(\rho^*, \theta)$ for any $\frac{H_\mathrm{s}}{H_\min} L\cos\theta > \rho_4 > \rho_3 > \rho^*$. Therefore, we can conclude that $F_k(\rho, \theta)$ is strictly quasiconvex in ρ for both Type I and Type II functions. In addition, from Proposition 4 proven in Appendix C, the optimal solution ρ^* is bounded in $0 \le \rho \le \frac{H_\mathrm{s}}{H_\min} L\cos\theta$. As a result, using Lemma 3, $F_k(\rho, \theta)$ admits a unique local minimizer $\rho^*(\theta)$ for each θ.

APPENDIX C
PROOF OF PROPOSITION 4

Denote the elevation angle as φ. Then, from geometric relation as illustrated in Fig. 11, we have $\cos\varphi = \frac{\rho}{\sqrt{\rho^2 + H_\mathrm{s}^2}}$ and $\sin\varphi = \frac{H_\mathrm{s}}{\sqrt{\rho^2 + H_\mathrm{s}^2}}$. As a result, (25) can be written as

$$\begin{aligned} D_\mathrm{b}(l, \rho, \theta) = L^2\sin^2\theta + (L\cos\theta - l\cos\varphi)^2 \\ +(l\sin\varphi - H_\mathrm{b})^2. \end{aligned}$$

The constraint in $\mathscr{P}'$ suggests that $H_\min \le l\sin\varphi \le H_\max$.

There are two cases for the optimal solution $l^*(\rho, \theta)$ discussed as follows.

(i) $l^*\sin\varphi > H_\min$: in this case, the following condition holds

$$\frac{\partial D_\mathrm{b}}{\partial l}\Big|_{l^*(\rho,\theta)} = 2(l - L\cos\theta\cos\varphi - H_\mathrm{b}\sin\varphi)\Big|_{l^*(\rho,\theta)} < 0$$

because otherwise, the gradient in $\mathscr{P}_k'$ becomes positive as

$$\begin{aligned} \frac{\partial \tilde{f}}{\partial l}\Big|_{l^*(\rho,\theta)} = \sum_{k=1}^{K} \Big(\frac{\partial f_k}{\partial d_\mathrm{b}}\frac{\partial d_\mathrm{b}}{\partial D_\mathrm{b}}\frac{\partial D_\mathrm{b}}{\partial l} + \frac{\partial f_k}{\partial d_\mathrm{u}}\frac{\partial D_\mathrm{u}}{\partial d_\mathrm{u}}\frac{\partial D_\mathrm{u}}{\partial l}\Big)\Big|_{l^*(\rho,\theta)} \\ \times\mathbb{I}\{\mathbf{x}(l, \rho, \theta) \in \mathcal{D}_k\} > 0 \end{aligned}$$

which means that $l^*(\rho, \theta)$ will not be the optimal solution. (Recall that f_k are increasing in the distances $d_\mathrm{b} = D_\mathrm{b}^{1/2}$ and $d_\mathrm{u} = D_\mathrm{u}^{1/2}$, and $D_\mathrm{u}(l) = l^2$). As a result, we have

$$\frac{H_\min}{\sin\varphi} \le l^* < L\cos\theta\cos\varphi - H_\mathrm{b}\sin\varphi$$

which arrives at

$$\begin{aligned} H_\min &< L\cos\theta\cos\varphi\sin\varphi + H_\mathrm{b}\sin^2\varphi \\ &= L\cos\theta\frac{\rho H_\mathrm{s} + H_\mathrm{b}H_\mathrm{s}^2}{\rho^2 + H_\mathrm{s}^2} \end{aligned}$$

leading to inequality

$$\rho^2 - \mu H_\mathrm{s}\rho + H_\mathrm{s}^2(1 - \mu H_\mathrm{b}) < 0 \tag{29}$$

where $\mu = L\cos\theta/H_\min$. Knowing that $\rho \ge 0$, we can solve (29) to obtain

$$\begin{aligned} \rho &< \frac{H_\mathrm{s}}{2}\Big(\mu + \sqrt{\mu^2 - 4(1 - \mu H_\mathrm{b})}\Big) \\ &< H_\mathrm{s}\mu = \frac{H_\mathrm{s}}{H_\min}L\cos\theta. \end{aligned}$$

(ii) $l^* \sin\varphi = H_{\min}$: in this case

$$D_{\rm b}^*(\rho,\theta) \triangleq D_{\rm b}(l^*(\rho,\theta),\rho,\theta) = L^2\sin^2\theta + (L\cos\theta - \rho\frac{H_{\min}}{H_{\rm s}})^2 + (H_{\min}-H_{\rm b})^2 \quad (30)$$

$$D_{\rm u}^*(\rho,\theta) \triangleq D_{\rm u}(l^*(\rho,\theta)) = \frac{H_{\min}^2}{H_{\rm s}^2}(\rho^2+H_{\rm s}^2). \quad (31)$$

Note that to fix the variable $l(\rho,\theta)$ as a pre-determined function of ρ and θ according to the relation $l\sin\varphi = H_{\min}$, minimizing $F_k(\rho,\theta)$ over $\rho \geq 0$ is an unconstrained problem. This is because $\rho \geq 0$ will be automatically satisfied as a result of (30)–(31). As a result, the optimality condition

$$\frac{\partial F_k}{\partial \rho} = \frac{\partial f_k}{\partial d_{\rm b}}\frac{\partial d_{\rm b}}{\partial D_{\rm b}^*}\frac{\partial D_{\rm b}^*}{\partial \rho} + \frac{\partial f_k}{\partial d_{\rm u}}\frac{\partial d_{\rm u}}{\partial D_{\rm u}^*}\frac{\partial D_{\rm u}^*}{\partial \rho} = 0$$

holds only if $\frac{\partial D_{\rm b}^*}{\partial \rho} < 0$, which leads to $\rho < \frac{H_{\rm s}}{H_{\min}} L\cos\theta$.

To conclude from the above two cases, the solution that minimizes $F_k(\rho,\theta)$ must satisfy $\rho^*(\theta) \leq \frac{H_{\rm s}}{H_{\min}} L\cos\theta$.

REFERENCES

[1] Y. Zeng, R. Zhang, and T. J. Lim, "Wireless communications with unmanned aerial vehicles: Opportunities and challenges," *IEEE Commun. Mag.*, vol. 54, no. 5, pp. 36–42, May 2016.

[2] M. Mozaffari, W. Saad, M. Bennis, and M. Debbah, "Unmanned aerial vehicle with underlaid device-to-device communications: Performance and tradeoffs," *IEEE Trans. Wireless Commun.*, vol. 15, no. 6, pp. 3949–3963, Jun. 2016.

[3] J. Lyu and R. Zhang, "Network-connected UAV: 3-D system modeling and coverage performance analysis," *IEEE Internet Things J.*, vol. 6, no. 4, pp. 7048–7060, Aug. 2019.

[4] A. Colpaert, E. Vinogradov, and S. Pollin, "Aerial coverage analysis of cellular systems at LTE and mmWave frequencies using 3D city models," *Sensors*, vol. 18, no. 12, p. 4311, Dec. 2018.

[5] M. Mozaffari, W. Saad, M. Bennis, Y.-H. Nam, and M. Debbah, "A tutorial on UAVs for wireless networks: Applications, challenges, and open problems," *IEEE Commun. Surveys Tuts.*, vol. 21, no. 3, pp. 2334–2360, 3rd Quart., 2019.

[6] X. Cao, P. Yang, M. Alzenad, X. Xi, D. Wu, and H. Yanikomeroglu, "Airborne communication networks: A survey," *IEEE J. Sel. Areas Commun.*, vol. 36, no. 9, pp. 1907–1926, Sep. 2018.

[7] M. M. Azari, F. Rosas, K.-C. Chen, and S. Pollin, "Ultra reliable UAV communication using altitude and cooperation diversity," *IEEE Trans. Commun.*, vol. 66, no. 1, pp. 330–344, Jan. 2018.

[8] Y. Zeng and R. Zhang, "Energy-efficient UAV communication with trajectory optimization," *IEEE Trans. Wireless Commun.*, vol. 16, no. 6, pp. 3747–3760, Jun. 2017.

[9] J. Chen and D. Gesbert, "Efficient local map search algorithms for the placement of flying relays," *IEEE Trans. Wireless Commun.*, vol. 19, no. 2, pp. 1305–1319, Feb. 2020.

[10] J. Chen, U. Mitra, and D. Gesbert, "Optimal UAV relay placement for single user capacity maximization over terrain with obstacles," in *Proc. IEEE 20th Int. Workshop Signal Process. Adv. Wireless Commun. (SPAWC)*, Jul. 2019, pp. 1–5.

[11] J. Lyu, Y. Zeng, R. Zhang, and T. J. Lim, "Placement optimization of UAV-mounted mobile base stations," *IEEE Commun. Lett.*, vol. 21, no. 3, pp. 604–607, Mar. 2017.

[12] V. V. Chetlur and H. S. Dhillon, "Downlink coverage analysis for a finite 3-D wireless network of unmanned aerial vehicles," *IEEE Trans. Commun.*, vol. 65, no. 10, pp. 4543–4558, Oct. 2017.

[13] Y. Zeng, R. Zhang, and T. J. Lim, "Throughput maximization for UAV-enabled mobile relaying systems," *IEEE Trans. Commun.*, vol. 64, no. 12, pp. 4983–4996, Dec. 2016.

[14] A. Hourani, K. Sithamparanathan, and S. Lardner, "Optimal LAP altitude for maximum coverage," *IEEE Wireless Commun. Lett.*, vol. 3 no. 6, pp. 569–572, Dec. 2014.

[15] M. Mozaffari, W. Saad, M. Bennis, and M. Debbah, "Efficient deployment of multiple unmanned aerial vehicles for optimal wireless coverage," *IEEE Commun. Lett.*, vol. 20, no. 8, pp. 1647–1650, Aug. 2016.

[16] M. Alzenad, A. El-Keyi, F. Lagum, and H. Yanikomeroglu, "3-D placement of an unmanned aerial vehicle base station (UAV-BS) for energy-efficient maximal coverage," *IEEE Wireless Commun. Lett.*, vol. 6, no. 4, pp. 434–437, Aug. 2017.

[17] A. Al-Hourani, S. Kandeepan, and A. Jamalipour, "Modeling air-to-ground path loss for low altitude platforms in urban environments," in *Proc. IEEE Global Commun. Conf.*, Dec. 2014, pp. 2898–2904.

[18] H. El Hammouti, M. Benjillali, B. Shihada, and M.-S. Alouini, "Learn-as-you-fly: A distributed algorithm for joint 3D placement and user association in multi-UAVs networks," *IEEE Trans. Wireless Commun.*, vol. 18, no. 12, pp. 5831–5844, Dec. 2019.

[19] B. Jiang, J. Yang, H. Xu, H. Song, and G. Zheng, "Multimedia data throughput maximization in Internet-of-Things system based on optimization of cache-enabled UAV," *IEEE Internet Things J.*, vol. 6, no. 2, pp. 3525–3532, Apr. 2019.

[20] C.-C. Lai, C.-T. Chen, and L.-C. Wang, "On-demand density-aware UAV base station 3D placement for arbitrarily distributed users with guaranteed data rates," *IEEE Wireless Commun. Lett.*, vol. 8, no. 3, pp. 913–916, Jun. 2019.

[21] M. Alzenad, A. El-Keyi, and H. Yanikomeroglu, "3-D placement of an unmanned aerial vehicle base station for maximum coverage of users with different QoS requirements," *IEEE Wireless Commun. Lett.*, vol. 7, no. 1, pp. 38–41, Feb. 2018.

[22] Y. Chen, W. Feng, and G. Zheng, "Optimum placement of UAV as relays," *IEEE Commun. Lett.*, vol. 22, no. 2, pp. 248–251, Feb. 2018.

[23] X. Mo, Y. Huang, and J. Xu, "Radio-map-based robust positioning optimization for UAV-enabled wireless power transfer," *IEEE Wireless Commun. Lett.*, vol. 9, no. 2, pp. 179–183, Feb. 2020.

[24] S. Zhang and R. Zhang, "Radio map based 3D path planning for cellular-connected UAV," 2019, *arXiv:1912.00021*. [Online]. Available: http://arxiv.org/abs/1912.00021

[25] M. T. Dabiri and S. M. S. Sadough, "Optimal placement of UAV-assisted free-space optical communication systems with DF relaying," *IEEE Commun. Lett.*, vol. 24, no. 1, pp. 155–158, Jan. 2020.

[26] Q. Feng, J. McGeehan, E. K. Tameh, and A. R. Nix, "Path loss models for air-to-ground radio channels in urban environments," in *Proc. IEEE 63rd Veh. Technol. Conf.*, vol. 6, May 2006, pp. 2901–2905.

[27] K. T. Herring, J. W. Holloway, D. H. Staelin, and D. W. Bliss, "Path-loss characteristics of urban wireless channels," *IEEE Trans. Antennas Propag.*, vol. 58, no. 1, pp. 171–177, Jan. 2010.

[28] J. Chen, U. Yatnalli, and D. Gesbert, "Learning radio maps for UAV-aided wireless networks: A segmented regression approach," in *Proc. IEEE Int. Conf. Commun. (ICC)*, May 2017, pp. 1–6.

[29] J. Chen, O. Esrafilian, D. Gesbert, and U. Mitra, "Efficient algorithms for air-to-ground channel reconstruction in UAV-aided communications," in *Proc. IEEE Globecom Workshops (GC Wkshps)*, Dec. 2017, pp. 1–6.

[30] J. Chen and U. Mitra, "Data clustering using matrix factorization techniques for wireless propagation map reconstruction," in *Proc. IEEE Stat. Signal Process. Workshop (SSP)*, Freiburg, Germany, Jun. 2018, pp. 856–860.

[31] R. U. Nabar, H. Bolcskei, and F. W. Kneubuhler, "Fading relay channels: Performance limits and space–time signal design," *IEEE J. Sel. Areas Commun.*, vol. 22, no. 6, pp. 1099–1109, Aug. 2004.

[32] J. N. Laneman, D. N. C. Tse, and G. W. Wornell, "Cooperative diversity in wireless networks: Efficient protocols and outage behavior," *IEEE Trans. Inf. Theory*, vol. 50, no. 12, pp. 3062–3080, Dec. 2004.

[33] T. Wang, A. Cano, G. B. Giannakis, and J. N. Laneman, "High-performance cooperative demodulation with decode- and-forward relays," *IEEE Trans. Commun.*, vol. 55, no. 7, pp. 1427–1438, Jul. 2007.

[34] P. Mogensen *et al.*, "LTE capacity compared to the Shannon bound," in *Proc. IEEE 65th Veh. Technol. Conf.-VTC-Spring*, Apr. 2007, pp. 1234–1238.

[35] Z. Liu, R. Sengupta, and A. Kurzhanskiy, "A power consumption model for multi-rotor small unmanned aircraft systems," in *Proc. Int. Conf. Unmanned Aircr. Syst. (ICUAS)*, Jun. 2017, pp. 310–315.

[36] *Technical Specification Group Radio Access Network; Evolved Universal Terrestrial Radio Access (E-UTRA); Further Advancements for E-UTRA Physical Layer Aspects*, document TR 36.814, 3GPP, 2010.

[37] M. R. Akdeniz *et al.*, "Millimeter wave channel modeling and cellular capacity evaluation," *IEEE J. Sel. Areas Commun.*, vol. 32, no. 6, pp. 1164–1179, Jun. 2014.

Junting Chen (Member, IEEE) received the B.Sc. degree in electronic engineering from Nanjing University, Nanjing, China, in 2009, and the Ph.D. degree in electronic and computer engineering from The Hong Kong University of Science and Technology (HKUST), Hong Kong, SAR, China, in 2015.

From 2014 to 2015, he was a Visiting Student with the Wireless Information and Network Sciences Laboratory, MIT, Cambridge, MA, USA. He is currently an Assistant Professor with the School of Science and Engineering and the Future Network of Intelligence Institute (FNii), The Chinese University of Hong Kong, Shenzhen (CUHK-Shenzhen), China. Prior to joining CUHK-Shenzhen, he was a Post-Doctoral Research Associate with the Ming Hsieh Department of Electrical Engineering, University of Southern California (USC), Los Angeles, CA, USA, from 2016 to 2018, and from 2015 to 2016, he was with the Department of Communication Systems, EURECOM, Sophia-Antipolis, France. He works on unimodal signal processing, radio map sensing, UAV assisted communications, and, more generally, machine learning and optimization for wireless communications and localization. He was a recipient of the HKTIIT Post-Graduate Excellence Scholarships in 2012 from HKUST.

Urbashi Mitra (Fellow, IEEE) received the B.S. and M.S. degrees from the University of California at Berkeley, Berkeley, CA, USA, and the Ph.D. degree from Princeton University, Princeton, NJ, USA. After a six-year stint with The Ohio State University, Columbus, OH, USA, she joined the Department of Electrical Engineering, University of Southern California, Los Angeles, CA, USA, where she is currently the Gordon S. Marshall Chair of Engineering. Her research interests include wireless communications, biological communication, underwater acoustic communications, communication and sensor networks, detection and estimation, and the interface of communication, sensing and control. She has served on the IEEE Fourier Award for Signal Processing, the IEEE James H. Mulligan, Jr. Education Medal, and the IEEE Paper Prize committees. She has Co-Chaired (technical program) of the 2018 IEEE International Workshop on Signal Processing Advances in Wireless Communications, Kalamata, Greece, the 2014 IEEE International Symposium on Information Theory, Honolulu, HI, USA, the 2014 IEEE Information Theory Workshop, Hobart, Tasmania, the IEEE 2012 International Conference on Signal Processing and Communications, Bangalore, India, and the IEEE Communication Theory Symposium at ICC 2003, Anchorage, AK, USA. She was the General Co-Chair of the first ACM Workshop on Underwater Networks at Mobicom 2006, Los Angeles, CA, USA, the Tutorials Chair of the IEEE ISIT 2007, Nice, France, and the Finance Chair of the IEEE ICASSP 2008, Las Vegas, NV, USA. She served as the Co-Director for the Communication Sciences Institute, University of Southern California, from 2004 to 2007. She was a recipient of the 1996 National Science Foundation (NSF) CAREER Award, the 1997 OSU College of Engineering MacQuigg Award for Teaching, the 2000 OSU College of Engineering Lumley Award for Research, the 2001 Okawa Foundation Award, the Texas Instruments Visiting Professorship (Fall 2002, Rice University), the Texas Instruments Visiting Professorship (Fall 2002, Rice University), the 2009 DCOSS Applications and Systems Best Paper Award, the 2012 Globecom Signal Processing for Communications Symposium Best Paper Award, the 2012 NAE Lillian Gilbreth Lectureship, the USC Center for Excellence in Research Fellowship (from 2010 to 2013), the IEEE Communications Society Distinguished Lecturer (from 2014 to 2015), the 2017 IEEE Communications Society Women in Communications Engineering Technical Achievement Award, the 2016 U.K. Royal Academy of Engineering Distinguished Visiting Professorship, the 2016 U.S. Fulbright Scholar Award, and the U.K. Leverhulme Trust Visiting Professorship (2016 to 2017). She is the inaugural Editor-in-Chief of the IEEE TRANSACTIONS ON MOLECULAR, BIOLOGICAL, AND MULTI-SCALE COMMUNICATIONS. She has been an Associate Editor of the IEEE TRANSACTIONS ON SIGNAL PROCESSING from 2012 to 2015, the IEEE TRANSACTIONS ON INFORMATION THEORY from 2007 to 2011, the IEEE JOURNAL OF OCEANIC ENGINEERING from 2006 to 2011, and the IEEE TRANSACTIONS ON COMMUNICATIONS from 1996 to 2001.

David Gesbert (Fellow, IEEE) received the Ph.D. degree from the Ecole Nationale Superieure des Telecommunications, France, in 1997. From 1997 to 1999, he was with the Information Systems Laboratory, Stanford University. He was then a Founding Engineer with Iospan Wireless Inc. and a Stanford spin off pioneering MIMO-OFDM (Intel). Before joining EURECOM in 2004, he was with the Department of Informatics, University of Oslo, as an Adjunct Professor. Since 2015, he holds the ERC Advanced grant "PERFUME" on the topic of smart device Communications in future wireless networks. He has published about 300 articles and 25 patents, some of them winning the 2019 ICC Best Paper Award, the 2015 IEEE Best Tutorial Paper Award (Communications Society), the 2012 SPS Signal Processing Magazine Best Paper Award, the 2004 IEEE Best Tutorial Paper Award (Communications Society), the 2005 Young Author Best Paper Award for Signal Processing Society journals, and paper awards at conferences 2011 IEEE SPAWC, 2004 ACM MSWiM. He is a Board Member of the OpenAirInterface (OAI) Software Alliance. He has been a Technical Program Co-chair of ICC2017. He was named a Thomson-Reuters Highly Cited Researchers in Computer Science. Since early 2019, he heads the Huawei-funded Chair on Adwanced Wireless Systems Towards 6G Networks. He sits on the Advisory Board of HUAWEI European Research Institute. In 2020, he was awarded funding by the French Interdisciplinary Institute on Artificial Intelligence for a Chair in the area of AI for the future IoT.